Nucleon relativistic weak-neutral axial-vector four-current distributions

Yi Chen[*]

Interdisciplinary Center for Theoretical Study and Department of Modern Physics,
University of Science and Technology of China, Hefei, Anhui 230026, China

Relativistic full weak-neutral axial-vector four-current distributions inside a general spin-$\frac{1}{2}$ system are systematically studied for the first time, where the second-class current contribution associated with the induced (pseudo-)tensor form factor (FF) is included. For experimental measurements, we explicitly derive the first exact full tree-level unpolarized differential cross sections of both (anti)neutrino-nucleon and (anti)neutrino-antinucleon elastic scatterings. We clearly demonstrate that the 3D axial charge distribution in the Breit frame, being purely imaginary and parity-odd, is in fact related to the induced (pseudo-)tensor FF $G_T^Z(Q^2)$ rather than the axial FF $G_A^Z(Q^2)$. We study the frame-dependence of full axial-vector four-current distributions for a moving system, and compared them with their light-front counterparts. We clarify the role played by Melosh rotations, and classify the origin of distortions in light-front distributions into three key sources using the lemma that we have proposed and verified in this work. In particular, we show that the second-class current contribution, although explicitly included, does not contribute in fact to the mean-square axial and spin radii. We finally illustrate our results in the case of a proton using the weak-neutral axial-vector FFs extracted from experimental data.

---

[*] physchen@mail.ustc.edu.cn

CONTENTS

I. INTRODUCTION

Nucleons (i.e. protons and neutrons) are key hadrons to study for understanding quantum chromodynamics (QCD), since they are responsible for more than 99% of the visible-matter mass in the universe [1]. Protons, in particular, also hold another unique role of being the only stable composite building blocks in nature [2]. Due to the complicated nonperturbative dynamics of their quark and gluon degrees of freedom, nucleons inherit particularly rich and intricate internal structures. Properties and internal structures of these key QCD bound-state systems in the weak sector become increasingly important when come to the experimental studies of nucleon axial-vector form factors (FFs) in high-energy elastic or quasielastic (anti)neutrino-(anti)nucleon scatterings [3–22].

Axial-vector FFs are Lorentz-invariant functions that describe how the hadron reacts with the incoming (anti)neutrino in a scattering reaction, encoding therefore very clean internal axial charge and spin information of the hadron in the weak sector since (anti)neutrinos participate only in weak interactions. In the Standard Model, there are in general two types of axial-vector FFs of a hadron in the weak sector: the weak-charged ones via the weak-charged current interactions mediated by the $W^{\pm}$ bosons, and the weak-neutral ones via the weak-neutral current interactions mediated by the Z^0 bosons. These axial-vector FFs also serve as important quantities for constraining the systematic uncertainties of high-precision measurements in (anti)neutrino oscillation experiments [23–31]. On the theory side, tremendous progress has been made in the last few years from first principle lattice QCD calculations of these axial-vector FFs [32–57]; theoretical evaluations of these axial-vector FFs and cross sections based on chiral perturbation theory and various models are still vividly developing [58–90]. For (recent) reviews of nucleon axial-vector FFs and associated physics of (anti)neutrino interactions, see e.g. Refs. [91–106].

According to textbooks, charge distributions can be defined in the Breit frame (BF) in term of three-dimensional (3D) Fourier transform of the Sachs electric FF [1, 107, 108]. However, relativistic recoil corrections spoil their interpretation as probabilistic distributions [109–114]. In position space, a probabilistic density interpretation is tied to Galilean symmetry that implies the invariance of inertia under the change of frames. In a relativistic theory, inertia becomes however a frame-dependent concept because of Lorentz symmetry. The only way out is to switch to the light-front (LF) formalism [115] where a Galilean sub-

group of the Lorentz group is singled out [116, 117], allowing therefore a nice probabilistic interpretation [118–128]. The price to pay is that besides losing the longitudinal spatial dimension[1], these LF distributions also exhibit various distortions owing to the particular LF perspective and the complicated Wigner-Melosh rotations [130–135], which are sometimes hard to reconcile with an intuitive picture of the system in 3D at rest.

The quantum phase-space formalism distinguishes itself by the fact that the requirement of a strict probabilistic interpretation is relaxed and replaced by a milder quasiprobabilistic picture [136–138]. This approach is quite appealing since it allows one to define in a consistent way relativistic spatial distributions inside a target with arbitrary spin and arbitrary average momentum [139–149], providing a smooth and neutral connection between the BF and essentially the LF pictures[2], and allowing one to explicitly trace the spatial distortions induced by Wigner rotations at arbitrary average momenta for any spin-j hadrons under the protection of Poincaré symmetry.

As a extension of our recent work [148], we study in this work in detail the frame-dependence of the relativistic weak-neutral axial-vector four-current distributions inside a general spin-$\frac{1}{2}$ hadron (the nucleon for instance), where the second-class current contribution associated with the induced (pseudo-)tensor FF $G_T^Z(Q^2)$ is *newly* taken into account in terms of full matrix elements. For ongoing and future experimental measurements and data analyses of elastic (anti)neutrino-(anti)nucleon scatterings [9, 10, 15, 18], we also derive the first exact full tree-level unpolarized differential cross sections of both (anti)neutrino-nucleon and (anti)neutrino-antinucleon elastic scatterings in the lab frame using the full vertex functions including 6 FFs individually.

We explicitly demonstrate that the relativistic 3D weak-neutral axial charge distribution in the BF, being purely imaginary and parity-odd, is in fact related to the weak-neutral induced (pseudo-)tensor FF $G_T^Z(Q^2)$ rather than the axial FF $G_A^Z(Q^2)$. For the derivations of LF amplitudes, we proposed and verified the following lemma: *Any light-front amplitudes for well-defined light-front distributions in principle can be explicitly reproduced from the corresponding elastic-frame amplitudes in the proper infinite-momentum-frame limit.* As a reward, we can classify more clearly the origin of distortions appearing in LF distributions

---

[1] We note that Miller and Brodsky [129] have recently demonstrated at the wavefunction level that frame-independent and three-dimensional LF coordinate-space wavefunctions can be obtained by using the dimensionless, frame-independent longitudinal coordinate $\tilde{z}$.

[2] Strictly speaking, the smooth connection is between the 2D BF and 2D infinite-momentum frame (IMF) distributions, see e.g., Refs. [142, 146–148]. However, IMF distributions coincide most of the time with the corresponding LF distributions [147].

in general into three key sources. For completeness, both 3D and 2D transverse mean-square axial and spin radii in different frames are explicitly rederived, where we show in particular that the second-class current contribution, although explicitly included in our calculations, does not contribute in fact to the mean-square axial and spin radii.

The paper is organized as follows. In Sec. II, we first briefly review the matrix elements of weak-neutral axial-vector and vector four-current operators and associated FFs for a general spin-$\frac{1}{2}$ hadron, and then derive the exact full tree-level unpolarized differential cross sections of both (anti)neutrino-nucleon and (anti)neutrino-antinucleon elastic scatterings in the lab frame for experimental measurements. In Sec. III, we present the key ingredients of the quantum phase-space formalism. We start our analysis in Sec. IV with the 3D Breit frame distributions of weak-neutral axial-vector four-current inside a spin-$\frac{1}{2}$ hadron. We then present in Sec. V the generic elastic frame distributions inside a moving spin-$\frac{1}{2}$ hadron at arbitrary average momenta. In Sec. VI, we present the light-front distributions, and the explicit demonstration of light-front amplitudes via the proper infinite-momentum frame limit of elastic-frame amplitudes. In Sec. IV to Sec. VI, we also supply our rederived 3D and 2D transverse mean-square axial and spin radii. Finally, we summarize our findings in Sec. VII. For completeness, we also provide details for the parametrization of nucleon weak-neutral axial-vector form factors in Appendix A, and further discussions on the breakdown of Abel transformation of axial charge distributions in Appendix B.

II.   ELASTIC (ANTI)NEUTRINO-(ANTI)NUCLEON SCATTERINGS

A.   Weak-neutral axial-vector four-current and FFs

The weak-neutral axial-vector FFs of a spin-$\frac{1}{2}$ hadron in the weak sector contain in general axial G_A^Z, induced pseudoscalar G_P^Z and induced (pseudo-)tensor G_T^Z FFs [61, 65, 92, 94], as *real* functions of spacelike four-momentum transfer squared $Q^2 = -\Delta^2 \geq 0$ owing to the time-reversal (T) invariance of weak interactions [62, 92]. They together describe the internal weak-neutral axial-vector content of the system in response to external weak-neutral current interactions; see e.g., Fig. 1 for the tree-level Feynman diagram of neutrino-nucleon elastic scattering.

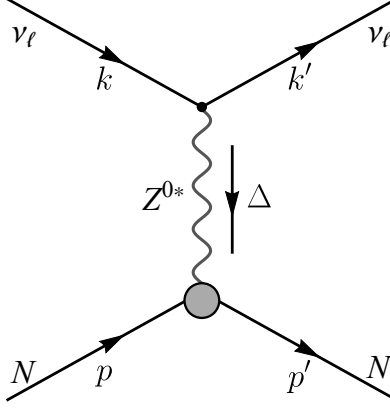In the case of a spin-$\frac{1}{2}$ hadron, matrix elements of the weak-neutral axial-vector four-

FIG. 1. The tree-level Feynman diagram of the t-channel weak-neutral current elastic scattering reaction $\nu_\ell(k) + N(p) \to \nu_\ell(k') + N(p')$ in the first Born approximation (i.e. one virtual Z^0 boson exchange), with $\ell = e, \mu, \tau$. The four-momentum transfer is $\Delta = k - k' = p' - p$.

current operator $\hat{j}_5^\mu(x) \equiv \hat{\bar\psi}(x)\gamma^\mu\gamma^5\hat\psi(x)$ in general can be parametrized as [61, 65, 92, 94]

$$\langle p', s'|\hat{j}_5^\mu(0)|p, s\rangle = \bar u(p', s')\left[\gamma^\mu G_A^Z + \frac{\Delta^\mu}{2M}G_P^Z + \frac{i\sigma^{\mu\nu}\Delta_\nu}{2M}G_T^Z\right]\gamma^5 u(p, s), \qquad (1)$$

where $\hat\psi(x)$ denotes the quark field operator (which can either be a flavor-singlet or flavor-multiplet), and $p^2 = p'^2 = M^2$ are the on-mass-shell relations for the same hadron B of mass M in the initial and final states. For better legibility, we have omitted the hadron index "B" attached to momentum-eigenstates, and the explicit Q^2-dependence of these weak-neutral axial-vector FFs $G_A^Z(Q^2)$, $G_P^Z(Q^2)$ and $G_T^Z(Q^2)$. Since the explicit (diagonal) matrix forms of generators T_a associated with the operator $\hat{j}_{5,a}^\mu(x) \equiv \hat{\bar\psi}(x)\gamma^\mu\gamma^5 T_a\hat\psi(x)$, see e.g. Ref. [94], for a given flavor-space fundamental representation group $SU(n)_f$ ($n \geq 2$ and $n \in \mathbb{Z}$) of a given (anti)neutrino-hadron elastic scattering reaction are known, it is convenient to work in the $U(1)_f$ representation without loss of generality.

According to Weinberg [150], one can use the G-parity to classify all possible currents formed by Dirac bilinears in the literature in term of the *first-* and *second-class* currents. The G-parity is defined as the combination of the charge-conjugation C-parity after an rotation of a 180° angle around the y-axis in isospin space, namely

$$\mathsf{G} \equiv \mathsf{C}\exp(i\pi I_y), \qquad (2)$$

where $I_y = \sigma_y/2$ is the y-component isospin matrix. As the *ne plus ultra*, one can easily

demonstrate that the vector and axial-vector four-currents $j^\mu = \bar{\psi}\gamma^\mu\psi$ and $j_5^\mu = \bar{\psi}\gamma^\mu\gamma^5\psi$ which transform in the following manner

$$\mathsf{G}j^\mu\mathsf{G}^{-1} = +j^\mu, \qquad \mathsf{G}j_5^\mu\mathsf{G}^{-1} = -j_5^\mu \tag{3}$$

are classified as the *first-class* currents, whereas those transform in the opposite manner

$$\mathsf{G}j^\mu\mathsf{G}^{-1} = -j^\mu, \qquad \mathsf{G}j_5^\mu\mathsf{G}^{-1} = +j_5^\mu \tag{4}$$

are classified as the *second-class* currents. For completeness, we do summarize in Table I the classification of all possible independent currents formed by Dirac bilinears under the G-parity transformation.

TABLE I. Classification of the *first-* and *second-class* currents formed by Dirac bilinears under the G-parity transformation, see e.g. Eqs. (3) and (4).

Type	Dirac bilinears	*first-class* currents	*second-class* currents
Scalar	$\bar{\psi}\psi$	$-\bar{\psi}\psi$	$+\bar{\psi}\psi$
Pseudoscalar	$\bar{\psi}\gamma^5\psi$	$-\bar{\psi}\gamma^5\psi$	$+\bar{\psi}\gamma^5\psi$
Vector	$\bar{\psi}\gamma^\mu\psi$	$+\bar{\psi}\gamma^\mu\psi$	$-\bar{\psi}\gamma^\mu\psi$
Axial-vector	$\bar{\psi}\gamma^\mu\gamma^5\psi$	$-\bar{\psi}\gamma^\mu\gamma^5\psi$	$+\bar{\psi}\gamma^\mu\gamma^5\psi$
Tensor	$\bar{\psi}i\sigma^{\mu\nu}\psi$	$+\bar{\psi}i\sigma^{\mu\nu}\psi$	$-\bar{\psi}i\sigma^{\mu\nu}\psi$

Using Weinberg's classification, we can thus identify G_A^Z and G_P^Z in Eq. (1) as the FFs associated with the first-class currents, while identify G_T^Z as the FF associated with the second-class current. Our analysis is well consistent with Refs. [61, 92]. In the presence of exact isospin symmetry or G-parity invariance, the second-class current contribution in Eq. (1) vanishes identically [61, 65, 94], i.e. $G_T^Z(Q^2) = 0$. Note also the fact that G-parity invariance is well respected by strong interactions or QCD, it is thus common in the literature that the second-class current contribution of a hadron in Eq. (1) is usually not much discussed and calculated, see e.g. Refs. [58–60, 63–85, 87].

B. Weak-neutral vector four-current and FFs

According to the famous $V - A$ theory [151–153] in weak interactions, there are two types of currents involved in both weak-neutral and weak-charged current interactions: the weak vector current $\hat{j}^\mu(x) \equiv \hat{\bar{\psi}}(x)\gamma^\mu\hat{\psi}(x)$ and the weak axial-vector current $\hat{j}_5^\mu(x) \equiv \hat{\bar{\psi}}(x)\gamma^\mu\gamma^5\hat{\psi}(x)$. They together celebrate in the $V - A$ form for the total weak current of the system:

$$\langle p', s'|[\hat{j}^\mu(0) - \hat{j}_5^\mu(0)]|p, s\rangle = \bar{u}(p', s')\Gamma_{V-A}^\mu(p', p)u(p, s), \tag{5}$$

where Γ_{V-A}^μ is the total vertex function. In the weak neutral sector, matrix elements of the axial-vector four-current operator for a general spin-$\frac{1}{2}$ target can be generically parametrized in the form of Eq. (1). Similarly, matrix elements of the weak-neutral vector four-current operator for a generic spin-$\frac{1}{2}$ target in general can be parametrized as [61, 142, 147, 154–156]

$$\langle p', s'|\hat{j}^\mu(0)|p, s\rangle = \bar{u}(p', s') \left[\frac{MP^\mu}{P^2}G_E^Z + \frac{i\epsilon^{\mu\alpha\beta\lambda}\Delta_\alpha P_\beta\gamma_\lambda\gamma^5}{2P^2}G_M^Z + \frac{\Delta^\mu}{2M}G_S^Z \right] u(p, s), \tag{6}$$

where $P = (p' + p)/2$, $\Delta = p' - p$, $p^2 = p'^2 = M^2$ and $\epsilon_{0123} = +1$. Likewise Eq. (1), we have also omitted the explicit Q^2-dependence for the weak-neutral vector FFs G_E^Z, G_M^Z and G_S^Z, where G_E^Z and G_M^Z are the weak-neutral electromagnetic FFs associated with the first-class currents, and G_S^Z is the weak-neutral induced scalar FF associated with the second-class current. If one imposes the hypothesis of conserved weak-neutral vector four-current (or the Ward identities of weak-neutral vector four-current quantum amplitudes) that also follows naturally from the Standard Model, it is evident that $G_S^Z(Q^2) = 0$ [156].

C. Exact full tree-level unpolarized differential cross sections

Since we have discussed the full vertex function (5) for a generic spin-$\frac{1}{2}$ hadron, we are now ready to connect these weak-neutral FFs G_E^Z, G_M^Z, G_S^Z, G_A^Z, G_P^Z and G_T^Z to the unpolarized differential cross sections measured in (anti)neutrino-nucleon elastic scattering experiments [9, 10, 15, 18]. It should be noted that although the tree-level unpolarized differential cross sections of (anti)neutrino-nucleon elastic scatterings have been derived in Refs. [9, 10, 157–160], the vertex function Γ_{V-A}^μ employed in Refs. [9, 10, 157–160] is however incomplete, missing usually the Lorentz structures associated with G_T^Z, G_S^Z and even G_P^Z.

For neutrino-nucleon elastic scattering reaction (with $\ell = e, \mu, \tau$)

$$\nu_\ell(k, r) + N(p, s) \to \nu_\ell(k', r') + N(p', s'), \tag{7}$$

the scattering amplitude $i\mathcal{M}$ in the Feynman gauge is given by

$$i\mathcal{M} = (-i\,\xi_C) \left(\frac{M_Z^2}{M_Z^2 + Q^2} \right) \frac{G_F}{\sqrt{2}} L_\mu J_{\text{weak}}^\mu, \tag{8}$$

with

$$L_\mu \equiv \bar{u}(k', r')\gamma_\mu(1 - \gamma^5)u(k, r),$$
$$J_{\text{weak}}^\mu \equiv \bar{u}(p', s')\Gamma_{V-A}^\mu u(p, s), \tag{9}$$

where $\xi_C = 1$ (for weak-neutral currents), $M_Z \approx 91.1880(20)$ GeV is the Z^0 boson mass [161], G_F is the Fermi coupling constant, Γ_{V-A}^μ is the full vertex function given in Eq. (5), and we have used the fact that

$$\frac{G_F}{\sqrt{2}} = \frac{g^2}{8M_Z^2 \cos^2 \theta_W}, \tag{10}$$

with g the universal weak coupling constant and θ_W the Weinberg angle.

We then proceed to obtain the following spin averaged and summed unpolarized scattering amplitude squared $\overline{|\mathcal{M}|^2}$, namely

$$\overline{|\mathcal{M}|^2} = \left(\frac{M_Z^2}{M_Z^2 + Q^2} \right)^2 \frac{G_F^2}{4} L_{\mu\nu} H^{\mu\nu}, \tag{11}$$

with

$$L_{\mu\nu} \equiv \text{tr}\left[(\slashed{k}' + m_{\nu_\ell})\gamma_\mu(1 - \gamma^5)(\slashed{k} + m_{\nu_\ell})(1 + \gamma^5)\gamma_\nu \right],$$
$$H^{\mu\nu} \equiv \text{tr}\left[(\slashed{p}' + M)\Gamma_{V-A}^\mu(\slashed{p} + M)\gamma^0\Gamma_{V-A}^{\nu\dagger}\gamma^0 \right], \tag{12}$$

where $s \equiv (k+p)^2$, $Q^2 = -(k-k')^2$, $k^2 = k'^2 = m_{\nu_\ell}^2$, and $p^2 = p'^2 = M^2$. One can check that the (anti)neutrino mass m_{ν_ℓ} in fact does *not* contribute to $L_{\mu\nu}$. For antineutrino scattering, we simply need to replace $L_{\mu\nu}$ as follows

$$L_{\mu\nu} \equiv \text{tr}\left[(\slashed{k} - m_{\nu_\ell})\gamma_\mu(1 - \gamma^5)(\slashed{k}' - m_{\nu_\ell})(1 + \gamma^5)\gamma_\nu \right]. \tag{13}$$

We are now ready to insert $\overline{|\mathcal{M}|^2}$ into the formula for the lab-frame tree-level unpolarized

differential cross section:

$$\frac{\mathrm{d}\sigma}{\mathrm{d}Q^2} = \frac{1}{16\pi(s-M^2)^2}\,\overline{|\mathcal{M}|^2} = \frac{G_F^2}{64\pi(s-M^2)^2}\left(\frac{M_Z^2}{M_Z^2+Q^2}\right)^2 L_{\mu\nu}H^{\mu\nu}. \tag{14}$$

As a result, the *exact* full tree-level unpolarized differential cross sections of the elastic scattering reactions $\nu_\ell(\bar{\nu}_\ell) + N \to \nu_\ell(\bar{\nu}_\ell) + N$ are explicitly obtained as follows:

$$\left.\frac{\mathrm{d}\sigma}{\mathrm{d}Q^2}\right|_{\nu_\ell(\bar{\nu}_\ell)-N} = \frac{G_F^2 M^2}{8\pi E_\nu^2}\left(\frac{M_Z^2}{M_Z^2+Q^2}\right)^2\left[A(Q^2) \pm \frac{s-u}{M^2}B(Q^2) + \frac{(s-u)^2}{M^4}C(Q^2)\right], \tag{15}$$

with

$$A \equiv 4\tau\left[(1+\tau)\left(G_A^Z\right)^2 + \tau\left(G_M^Z\right)^2 - \left(G_E^Z\right)^2 - \tau(1+\tau)\left(G_T^Z\right)^2\right],$$

$$B \equiv 4\tau G_A^Z G_M^Z, \tag{16}$$

$$C \equiv \frac{1}{4(1+\tau)}\left[(1+\tau)\left(G_A^Z\right)^2 + \tau\left(G_M^Z\right)^2 + \left(G_E^Z\right)^2 + \tau(1+\tau)\left(G_T^Z\right)^2\right],$$

where the $(-)+$ sign is for the (anti)neutrino-nucleon scattering, and explicit Q^2 dependence of these FFs $G_E^Z(Q^2)$, $G_M^Z(Q^2)$, $G_S^Z(Q^2)$, $G_A^Z(Q^2)$, $G_P^Z(Q^2)$, $G_T^Z(Q^2)$ for clarity is omitted. We note that M is the nucleon mass, E_ν is the incident (anti)neutrino energy in the lab frame, $Q^2 = 2MT = -\Delta^2$ is the reconstructed four-momentum transfer squared (with T the sum of kinetic energies of final-state nucleons), $\tau \equiv Q^2/(4M^2)$ and $s - u = 4ME_\nu - Q^2$. In particular, we observed that the terms associated with the FFs G_P^Z and G_S^Z in Eqs. (1) and (6), although explicitly included in our derivations, do not contribute in fact to the tree-level unpolarized differential cross sections (15).

Similarly for the neutrino-antinucleon elastic scattering reaction

$$\nu_\ell(k,r) + \bar{N}(p,s) \to \nu_\ell(k',r') + \bar{N}(p',s'), \tag{17}$$

we can simply replace $H^{\mu\nu}$ in Eq. (12) as follows

$$H^{\mu\nu} \equiv \mathrm{tr}\left[(\not{p} - M)\bar{\Gamma}_{V-A}^\mu(\not{p}' - M)\gamma^0\bar{\Gamma}_{V-A}^{\nu\dagger}\gamma^0\right], \tag{18}$$

with the full vertex function $\bar{\Gamma}_{V-A}^\mu$ given by

$$_{\bar{\mathrm{B}}}\langle p',s'|[\hat{j}^\mu(0) - \hat{j}_5^\mu(0)]|p,s\rangle_{\bar{\mathrm{B}}} = \bar{v}(p,s)\bar{\Gamma}_{V-A}^\mu v(p',s'), \tag{19}$$

with

$$_{\bar{\mathrm{B}}}\langle p', s'|\hat{j}^\mu(0)|p, s\rangle_{\bar{\mathrm{B}}} = \bar{v}(p, s) \left[-\frac{MP^\mu}{P^2}\bar{G}_E^Z + \frac{i\epsilon^{\mu\alpha\beta\lambda}P_\alpha\Delta_\beta\gamma_\lambda\gamma^5}{2P^2}\bar{G}_M^Z + \frac{\Delta^\mu}{2M}\bar{G}_S^Z \right] v(p', s'),$$
$$_{\bar{\mathrm{B}}}\langle p', s'|\hat{j}_5^\mu(0)|p, s\rangle_{\bar{\mathrm{B}}} = \bar{v}(p, s) \left[\gamma^\mu\bar{G}_A^Z + \frac{\Delta^\mu}{2M}\bar{G}_P^Z + \frac{i\sigma^{\mu\nu}\Delta_\nu}{2M}\bar{G}_T^Z \right] \gamma^5 v(p', s'),$$

(20)

where $|p, s\rangle_{\bar{\mathrm{B}}}$ is the canonical momentum eigenstates for the spin-$\frac{1}{2}$ antiparticle $\bar{\mathrm{B}}$ with $\bar{v}(p, s)$ the corresponding Dirac spinor in the initial state, and $\bar{G}_E^Z$, $\bar{G}_M^Z$, $\bar{G}_S^Z$, $\bar{G}_A^Z$, $\bar{G}_P^Z$, $\bar{G}_T^Z$ are the corresponding weak-neutral FFs of this antiparticle where explicit Q^2-dependence is omitted.

As a result, the *exact* full tree-level unpolarized differential cross sections of the elastic scattering reactions $\nu_\ell(\bar{\nu}_\ell) + \bar{N} \to \nu_\ell(\bar{\nu}_\ell) + \bar{N}$ are given by

$$\left.\frac{\mathrm{d}\sigma}{\mathrm{d}Q^2}\right|_{\nu_\ell(\bar{\nu}_\ell)-\bar{N}} = \frac{G_F^2 M^2}{8\pi E_\nu^2}\left(\frac{M_Z^2}{M_Z^2 + Q^2}\right)^2 \left[\bar{A}(Q^2) \pm \frac{s - u}{M^2}\bar{B}(Q^2) + \frac{(s - u)^2}{M^4}\bar{C}(Q^2)\right],$$

(21)

with

$$\bar{A} \equiv 4\tau\left[(1 + \tau)\left(\bar{G}_A^Z\right)^2 + \tau\left(\bar{G}_M^Z\right)^2 - \left(\bar{G}_E^Z\right)^2 - \tau(1 + \tau)\left(\bar{G}_T^Z\right)^2\right],$$
$$\bar{B} \equiv -4\tau\bar{G}_A^Z\bar{G}_M^Z,$$
$$\bar{C} \equiv \frac{1}{4(1 + \tau)}\left[(1 + \tau)\left(\bar{G}_A^Z\right)^2 + \tau\left(\bar{G}_M^Z\right)^2 + \left(\bar{G}_E^Z\right)^2 + \tau(1 + \tau)\left(\bar{G}_T^Z\right)^2\right],$$

(22)

where the $(-) +$ sign is for the (anti)neutrino-antinucleon scattering. In comparison with the differential cross sections (15) for the nucleon, the key difference of the differential cross sections (21) for the antinucleon lies in the extra minus sign for the definition of $\bar{B}(Q^2)$.

It should be emphasized that our exact results of the full tree-level unpolarized differential cross sections (15, 21) also apply to other spin-$\frac{1}{2}$ hadrons (including their antiparticles), e.g. Λ^0, $\bar{\Lambda}^0$, Σ^0, $\bar{\Sigma}^0$, Ξ^0, $\bar{\Xi}^0$, etc., where the full vertex functions (5, 19) including 6 FFs individually are explicitly taken into account. Relative to those previous studies [9, 10, 157–160], our results (15) of the full tree-level unpolarized differential cross sections are more general and complete, and should be more useful for ongoing and future elastic (anti)neutrino-nucleon scattering experiments [9, 10, 15, 18].

Last but not least, we *did* realize during the derivations of the full tree-level unpolarized differential cross sections (15, 21) that polarized differential cross sections of polarized (anti)neutrino-(anti)nucleon elastic scatterings will provide us more rich and complete information about nucleon weak-neutral vector and axial-vector FFs in the weak sector, where

FFs G_P^Z (or $\bar{G}_P^Z$) and G_S^Z (or $\bar{G}_S^Z$) may explicitly appear in the polarized differential cross sections[3], which may enable us to measure these 6 weak-neutral FFs individually in future experiments.

III. QUANTUM PHASE-SPACE FORMALISM

Although FFs are objects defined in momentum space and extracted from experimental data involving particles with well-defined momenta, their physical interpretation actually resides in position space [147]. Because of Lorentz symmetry, the notion of relativistic spatial distributions in general depends on the target average momentum, hindering therefore in general a probabilistic interpretation in position space. We are therefore naturally led to switch our perspective to a phase-space picture, which is *quasi*probabilistic at the quantum level owing to Heisenberg's uncertainty principle. In this section, we only present the key ingredients of the quantum phase-space formalism [142, 146, 147].

In quantum field theory, it has been known for a long time that the expectation value of any an operator $\hat{O}$ in a physical state $|\Psi\rangle$ can be expressed as [136–138]

$$\langle\Psi|\hat{O}(x)|\Psi\rangle = \sum_{s',s} \int \frac{\mathrm{d}^3 P}{(2\pi)^3}\, \mathrm{d}^3 R\, \rho_\Psi^{s's}(\boldsymbol{R},\boldsymbol{P})\, \langle\hat{O}\rangle_{\boldsymbol{R},\boldsymbol{P}}^{s's}(x), \tag{23}$$

where

$$\begin{aligned}
\rho_\Psi^{s's}(\boldsymbol{R},\boldsymbol{P}) &\equiv \int \mathrm{d}^3 z\, e^{-i\boldsymbol{P}\cdot\boldsymbol{z}}\, \Psi^*(\boldsymbol{R} - \tfrac{\boldsymbol{z}}{2}, s')\Psi(\boldsymbol{R} + \tfrac{\boldsymbol{z}}{2}, s) \\
&= \int \frac{\mathrm{d}^3 q}{(2\pi)^3}\, e^{-i\boldsymbol{q}\cdot\boldsymbol{R}}\, \widetilde{\Psi}^*(\boldsymbol{P} + \tfrac{\boldsymbol{q}}{2}, s')\widetilde{\Psi}(\boldsymbol{P} - \tfrac{\boldsymbol{q}}{2}, s)
\end{aligned} \tag{24}$$

defines the *Wigner distribution* interpreted as the quantum weight for finding the system at average position $\boldsymbol{R} = \frac{1}{2}(\boldsymbol{r}' + \boldsymbol{r})$ and average momentum $\boldsymbol{P} = \frac{1}{2}(\boldsymbol{p}' + \boldsymbol{p})$. Here, $\boldsymbol{z} \equiv \boldsymbol{r} - \boldsymbol{r}'$ and $\boldsymbol{q} \equiv \boldsymbol{p}' - \boldsymbol{p}$ denote the relative position and relative momentum, respectively.

We note that $\widetilde{\Psi}(\boldsymbol{p}, s) \equiv \langle p, s|\Psi\rangle/\sqrt{2p^0}$ defines the momentum-space wavepacket of the system, and satisfies the following completeness condition

$$\sum_s \int \frac{\mathrm{d}^3 p}{(2\pi)^3}\, |\widetilde{\Psi}(\boldsymbol{p}, s)|^2 = 1, \tag{25}$$

---

[3] We note that two virtual Z^0 bosons exchange (or multiple virtual Z^0 bosons exchange) and radiative corrections at one-loop order (or even higher loops) may also provide us the possibilities that nucleon FFs G_P^Z (or $\bar{G}_P^Z$) and G_S^Z (or $\bar{G}_S^Z$) may explicitly appear in the unpolarized differential cross sections.

where $|p, s\rangle$ denote the four-momentum eigenstates and are covariantly normalized as $\langle p', s'|p, s\rangle = 2p^0 (2\pi)^3 \delta^{(3)}(\boldsymbol{p}' - \boldsymbol{p}) \delta_{s's}$. Both initial and final four-momenta being on-mass-shell $p^2 = p'^2 = M^2$, the energy components are given by $p^0 = \sqrt{\boldsymbol{p}^2 + M^2}$ and $p'^0 = \sqrt{\boldsymbol{p}'^2 + M^2}$.

Accordingly, $\Psi(\boldsymbol{r}, s) \equiv \langle \boldsymbol{r}, s|\Psi\rangle$ defines the position-space wave packet at $t = 0$ via the Newton-Wigner position operator [162–165], whose eigenstates at $t = 0$ are related to momentum eigenstates via Fourier transforms

$$|\boldsymbol{r}, s\rangle = \int \frac{\mathrm{d}^3 p}{(2\pi)^3} \, e^{-i\boldsymbol{p}\cdot\boldsymbol{r}} \frac{|p, s\rangle}{\sqrt{2p^0}} \tag{26}$$

and are normalized as $\langle \boldsymbol{r}', s'|\boldsymbol{r}, s\rangle = \delta^{(3)}(\boldsymbol{r}' - \boldsymbol{r}) \delta_{s's}$. One finds that the position-space wave packet at $t = 0$ is related to the momentum-space one via the familiar Fourier transform

$$\Psi(\boldsymbol{r}, s) = \int \frac{\mathrm{d}^3 p}{(2\pi)^3} \, e^{i\boldsymbol{p}\cdot\boldsymbol{r}} \, \widetilde{\Psi}(\boldsymbol{p}, s) \tag{27}$$

and satisfies the following completeness condition

$$\sum_s \int \mathrm{d}^3 r \, |\Psi(\boldsymbol{r}, s)|^2 = 1. \tag{28}$$

In a relativistic theory, the Newton-Wigner position operator [162–165] is, to the best of our knowledge, the only 3D position operator satisfying usual commutation relations with both linear and angular momentum operators, and having mutually commuting components [140, 143]. Although this operator does not transform as part of a Lorentz four-vector, it allows one to localize a relativistic system at a fixed time. Probabilistic densities are then recovered upon integration over either average position or momentum variables

$$\int \mathrm{d}^3 R \, \rho_\Psi^{s's}(\boldsymbol{R}, \boldsymbol{P}) = \widetilde{\Psi}^*(\boldsymbol{P}, s') \widetilde{\Psi}(\boldsymbol{P}, s),$$
$$\int \frac{\mathrm{d}^3 P}{(2\pi)^3} \, \rho_\Psi^{s's}(\boldsymbol{R}, \boldsymbol{P}) = \Psi^*(\boldsymbol{R}, s') \Psi(\boldsymbol{R}, s). \tag{29}$$

A compelling feature of the quantum phase-space formalism is that wave-packet details have been cleanly factored out in Eq. (23). We can then interpret the phase-space amplitude

$$\langle \hat{O} \rangle_{\boldsymbol{R}, \boldsymbol{P}}^{s's}(x) = \int \frac{\mathrm{d}^3 \Delta}{(2\pi)^3} \, e^{i\boldsymbol{\Delta}\cdot\boldsymbol{R}} \frac{\langle P + \frac{\Delta}{2}, s'|\hat{O}(x)|P - \frac{\Delta}{2}, s\rangle}{2\sqrt{p'^0 p^0}} \tag{30}$$

as the *internal distribution* associated with a state localized in the Wigner sense around average position $\boldsymbol{R}$ and average momentum $\boldsymbol{P}$ [140–143, 146, 147], with $P \cdot \Delta = 0$.

IV.   BREIT FRAME DISTRIBUTIONS

From a phase-space perspective, the BF can be regarded as the average rest frame of the system, where spin structure assumes its simplest form [83, 142, 144, 147, 148]. In this frame, one can provide fully relativistic 3D spatial distributions of a generic composite system for its static internal structures in the Wigner sense. This is also the reason why many 3D mean-square radii of a hadron, e.g. (electric) charge $\langle r_{\text{ch}}^2 \rangle$, mass $\langle r_{\text{mass}}^2 \rangle$, mechanical $\langle r_{\text{mech}}^2 \rangle$ and spin $\langle r_{\text{spin}}^2 \rangle$ radii, are usually defined in this frame [1, 147, 148, 166–169].

The BF is specified by the condition $\boldsymbol{P} = \boldsymbol{0}$, which physically constrains that the energy transfer $\Delta^0 = \boldsymbol{P} \cdot \boldsymbol{\Delta}/P^0$ vanishes automatically in this frame. As a result, internal distributions in the BF do not dependent on time x^0 arising due to translation invariance of the matrix elements in Eq. (30). Relativistic three-dimensional BF distributions are therefore in general defined as [147]

$$O_B(\boldsymbol{r}) \equiv \langle \hat{O} \rangle_{\boldsymbol{0},\boldsymbol{0}}^{s_B' s_B}(\boldsymbol{r}) = \int \frac{\mathrm{d}^3 \Delta}{(2\pi)^3}\, e^{-i\boldsymbol{\Delta}\cdot\boldsymbol{r}}\, \frac{\langle p_B', s_B' | \hat{O}(0) | p_B, s_B \rangle}{2P_B^0}, \tag{31}$$

where $\boldsymbol{r} = \boldsymbol{x} - \boldsymbol{R}$ is the distance relative to the center $\boldsymbol{R} = \boldsymbol{0}$ of the system, $\boldsymbol{p}_B' = -\boldsymbol{p}_B = \boldsymbol{\Delta}/2$, $Q^2 = \boldsymbol{\Delta}^2$, $\tau \equiv Q^2/(4M^2)$ and $P_B^0 = p_B'^0 = p_B^0 = M\sqrt{1+\tau}$.

A.   BF weak-neutral axial-vector four-current distributions

Evaluating the matrix elements (1) in the BF leads to [59, 61, 62, 64, 148]

$$\begin{aligned}
\mathcal{A}_B^0 &= \sqrt{1+\tau}\,(\boldsymbol{\sigma} \cdot \boldsymbol{\Delta}) G_T^Z(\boldsymbol{\Delta}^2), \\
\boldsymbol{\mathcal{A}}_B &= 2P_B^0 \left[\boldsymbol{\sigma} - \frac{\boldsymbol{\Delta}(\boldsymbol{\Delta} \cdot \boldsymbol{\sigma})}{4P_B^0(P_B^0 + M)} \right] G_A^Z(\boldsymbol{\Delta}^2) - \frac{\boldsymbol{\Delta}(\boldsymbol{\Delta} \cdot \boldsymbol{\sigma})}{2M} G_P^Z(\boldsymbol{\Delta}^2),
\end{aligned} \tag{32}$$

where $\mathcal{A}_B^\mu \equiv \langle p_B', s_B' | \hat{j}_5^\mu(0) | p_B, s_B \rangle$, and explicit canonical polarization indices will be omitted for better legibility hereafter unless necessary.

Applying the general definition (31) to the axial-vector four-current operator with the

help of BF amplitudes (32), one obtains the following relativistic 3D BF weak-neutral axial-vector four-current distributions [148]

$$
\begin{aligned}
J_{5,B}^0(\boldsymbol{r}) &= \int \frac{\mathrm{d}^3\Delta}{(2\pi)^3}\, e^{-i\boldsymbol{\Delta}\cdot\boldsymbol{r}}\, \frac{\boldsymbol{\sigma}\cdot\boldsymbol{\Delta}}{2M} G_T^Z(\boldsymbol{\Delta}^2) = i\frac{\boldsymbol{\sigma}\cdot\boldsymbol{\nabla_r}}{2M} \int \frac{\mathrm{d}^3\Delta}{(2\pi)^3}\, e^{-i\boldsymbol{\Delta}\cdot\boldsymbol{r}}\, G_T^Z(\boldsymbol{\Delta}^2), \\
\boldsymbol{J}_{5,B}(\boldsymbol{r}) &= \int \frac{\mathrm{d}^3\Delta}{(2\pi)^3}\, e^{-i\boldsymbol{\Delta}\cdot\boldsymbol{r}}\left\{ \left[\boldsymbol{\sigma} - \frac{\boldsymbol{\Delta}(\boldsymbol{\Delta}\cdot\boldsymbol{\sigma})}{4P_B^0(P_B^0+M)}\right] G_A^Z(\boldsymbol{\Delta}^2) - \frac{\boldsymbol{\Delta}(\boldsymbol{\Delta}\cdot\boldsymbol{\sigma})}{4MP_B^0} G_P^Z(\boldsymbol{\Delta}^2)\right\}.
\end{aligned}
\tag{33}
$$

We do observe that the 3D BF axial charge distribution $J_{5,B}^0(\boldsymbol{r})$ is in fact related to the weak-neutral induced (pseudo-)tensor FF $G_T^Z(Q^2)$ rather than the axial FF $G_A^Z(Q^2)$. We stress that above results (32,33) are also well consistent with our previous work [148], where the G-parity invariance of QCD[4] (or exact isospin symmetry) is further applied to the matrix elements (1), eliminating therefore the second-class current contribution associated with the induced (pseudo-)tensor FF $G_T^Z(Q^2)$ [61, 65, 94].

The Fourier transform of $\boldsymbol{\Delta}G_T^Z(\boldsymbol{\Delta}^2)$ in Eq. (33) will lead to a purely imaginary BF axial charge distribution $J_{5,B}^0(\boldsymbol{r})$, since $G_T^Z(Q^2)$ is real by assuming the T-invariance of weak interactions [62, 91, 92, 155]. Besides, $J_{5,B}^0(\boldsymbol{r})$ is also parity-odd along the polarization axial owing to the associated parity-odd factor $(\boldsymbol{\sigma}\cdot\boldsymbol{r})$ coming from the Fourier transform of $(\boldsymbol{\sigma}\cdot\boldsymbol{\Delta})$. In Fig. 2, we illustrate the BF axial charge distributions $iJ_{5,B}^0(\boldsymbol{r}) = -\mathrm{Im}\left[J_{5,B}^0(\boldsymbol{r})\right]$ and $4\pi r^2 \cdot iJ_{5,B}^0(\boldsymbol{r})$ with $r = |\boldsymbol{r}|$ along the z-axis inside a longitudinally polarized proton, using proton's weak-neutral induced (pseudo-)tensor FF $G_T^Z(Q^2)$ given in Appendix A. For more details of the nucleon weak-neutral axial-vector FFs, see Appendix A.

On the other hand, we notice that the 3D BF axial-vector current distribution $\boldsymbol{J}_{5,B}$ is in fact independent of the induced tensor form factor $G_T^Z(Q^2)$. In other words, $\boldsymbol{J}_{5,B}$ is free from the second-class current contribution, and therefore assumes the same expression as in Ref. [148]. Using the QCD equation of motion [171], one can show that [139, 148]

$$
\boldsymbol{S}_B(\boldsymbol{r}) = \frac{1}{2}\boldsymbol{J}_{5,B}(\boldsymbol{r})
\tag{34}
$$

is the physically meaningful 3D spin distribution in the BF, characterizing how the spin is distributed in the weak neutral sector. Based on this meaningful and well-defined spin distribution (34), one can derive the meaningful 3D mean-square spin radius $\langle r_{\mathrm{spin}}^2\rangle$ [148],

---

[4] In strong interactions or QCD, e.g. the strong decays of mesons, the G-parity invariance is exact. However, the G-parity is in general not conserved in electromagnetic and weak interactions due to either quark mass or quark (electric) charge differences [170].
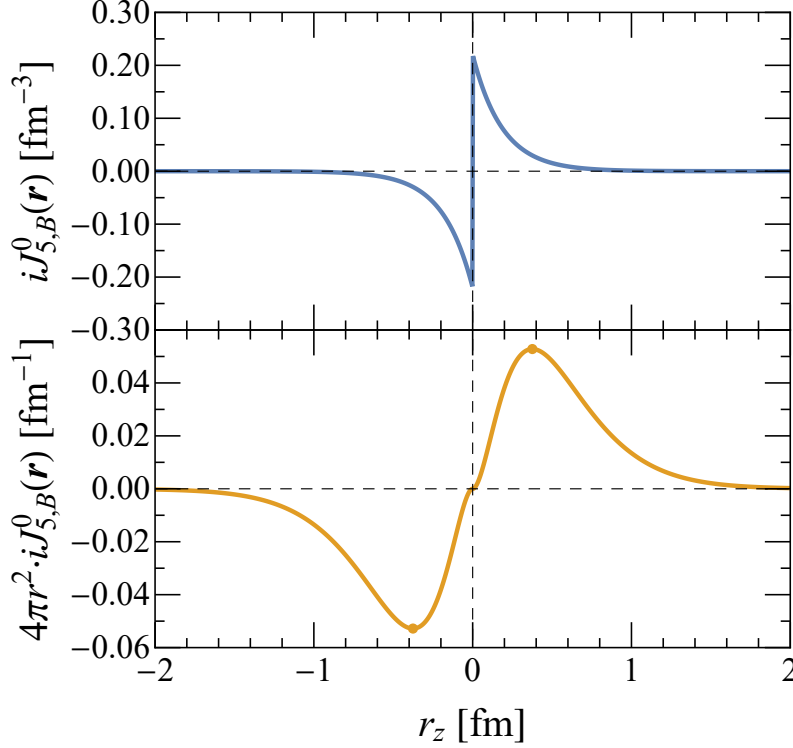
FIG. 2. BF weak-neutral axial charge distributions $iJ_{5,B}^0(\boldsymbol{r}) = -\text{Im}[J_{5,B}^0(\boldsymbol{r})]$ (upper panel) and $4\pi r^2 \cdot iJ_{5,B}^0(\boldsymbol{r})$ (lower panel) along the z-axis inside a longitudinally polarized (i.e. $\hat{\boldsymbol{s}} \equiv \boldsymbol{\sigma}_{s's} = \boldsymbol{e}_z$) proton, using proton's weak-neutral induced (pseudo-)tensor FF $G_T^Z(Q^2)$ given in Appendix A.

which relies on both the slope of the axial FF $G_A^Z(Q^2)$ at $Q^2 = 0$ and the ratio $G_P^Z(0)/G_A^Z(0)$. Using proton's weak-neutral axial-vector FFs $G_A^Z(Q^2)$ and $G_P^Z(Q^2)$ given in Appendix A, we find that the weak-neutral mean-square spin radius of the proton is given by [148]

$$\langle r_{\text{spin}}^2 \rangle^p = \frac{1}{G_A^Z(0)}\left[-\boldsymbol{\nabla}_{\boldsymbol{\Delta}}^2 G_A^Z(\boldsymbol{\Delta}^2)\right]\bigg|_{\boldsymbol{\Delta}=\boldsymbol{0}} + \frac{1}{4M^2}\left[1 + \frac{2G_P^Z(0)}{G_A^Z(0)}\right] \equiv r_S^2 \approx (2.1054\ \text{fm})^2, \quad (35)$$

where the last term $\left(\frac{1}{2M^2}\frac{G_P^Z(0)}{G_A^Z(0)}\right)$ plays the dominant role since the ratio $G_P^Z(0)/G_A^Z(0) = (2M_p/M_\pi)^2 \approx 180.772$ is very large; see Appendix A for more details of $G_A^Z(Q^2)$ and $G_P^Z(Q^2)$.

In Fig. 3, we illustrate the 3D BF weak-neutral axial-vector current distribution $\boldsymbol{J}_{5,B}(\boldsymbol{r})$ in the transverse plane inside a transversely polarized proton, using proton's weak-neutral axial-vector FFs $G_A^Z(Q^2)$ and $G_P^Z(Q^2)$ given in Appendix A. We observe that the distribution is perfectly mirror symmetric (antisymmetric) with respect to the x-axis (y-axis) in the transverse plane. This can be more easily understood from the multipole decomposition [147] of $\boldsymbol{J}_{5,B}(\boldsymbol{r})$, where we find that $\boldsymbol{J}_{5,B}(\boldsymbol{r})$ consists of mirror symmetric (antisymmetric) monopole
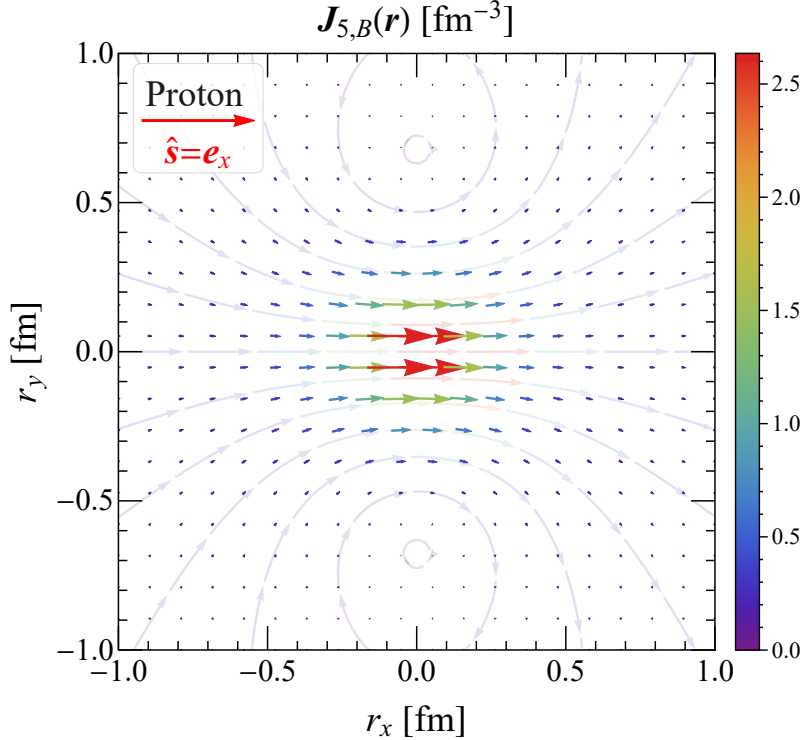
FIG. 3. The BF weak-neutral axial-vector current distribution $\boldsymbol{J}_{5,B}(\boldsymbol{r})$ in the transverse plane inside a transversely polarized (i.e. $\hat{\boldsymbol{s}} = \boldsymbol{e}_x$) proton, using proton's weak-neutral axial-vector FFs $G_A^Z(Q^2)$ and $G_P^Z(Q^2)$ given in Appendix A.

and quadrupole contributions solely with respect to the x-axis (y-axis).

Recalling in the BF that $\boldsymbol{p}'_B = -\boldsymbol{p}_B = \boldsymbol{\Delta}/2$ and $p'^0_B = p^0_B = P^0_B$, we do recognize in Eq. (32) the characteristic spin structure $\left(\boldsymbol{\sigma} - \frac{\boldsymbol{p}_B(\boldsymbol{p}_B \cdot \boldsymbol{\sigma})}{p^0_B(p^0_B + M)}\right)$ defined relative to the center of mass $\boldsymbol{R}_M = \boldsymbol{R} = \boldsymbol{0}$, which is the only relativistic center transforming as the spatial part of a Lorentz four-vector, and corresponds therefore to the *true* relativistic center of the system [140, 143, 147]. The other two relativistic centers are the center of energy $\boldsymbol{R}_E = \boldsymbol{R}_M + \frac{\boldsymbol{P} \times \hat{\boldsymbol{s}}}{2M(E_P + M)}$ and the center of canonical spin $\boldsymbol{R}_c = \boldsymbol{R}_M + \frac{\boldsymbol{P} \times \hat{\boldsymbol{s}}}{2ME_P}$ (the pivot about which the internal angular momentum takes the same value as in the rest frame), where $E_P \equiv \sqrt{\boldsymbol{P}^2 + M^2}$ and $\hat{\boldsymbol{s}}$ is a unit polarization vector. These two relativistic centers $\boldsymbol{R}_E$ and $\boldsymbol{R}_c$, however, will suffer from respectively sideways shifts $\frac{\boldsymbol{P} \times \hat{\boldsymbol{s}}}{2M(E_P + M)}$ and $\frac{\boldsymbol{P} \times \hat{\boldsymbol{s}}}{2ME_P}$ of pure relativistic origin when $(\boldsymbol{P} \times \hat{\boldsymbol{s}}) \neq \boldsymbol{0}$, e.g, when the spinning system is longitudinally moving while it is transversely polarized. This in turn justifies that the parametrization of the axial-vector four-current operator in Eq. (1) is *indeed* physically clear and transparent. For more details of the relativistic centers and sideways shifts, see Refs. [140, 143] and also the similar discussions for the parametrization of polarization-magnetization tensor in Ref. [147].

B. BF mean-square radii

Note that the total axial charge for a generic spin-$\frac{1}{2}$ composite system in average at rest vanishes identically [148]:

$$\int \mathrm{d}^3 r \, J_{5,B}^0(\boldsymbol{r}) = \lim_{\boldsymbol{\Delta} \to \boldsymbol{0}} \frac{1}{2M} \left[(\boldsymbol{\sigma} \cdot \boldsymbol{\Delta}) G_T^Z(\boldsymbol{\Delta}^2) \right] = 0, \tag{36}$$

because the term $(\boldsymbol{\sigma} \cdot \boldsymbol{\Delta})$ in momentum-space is parity-odd, or equivalently the term $(\boldsymbol{\sigma} \cdot \boldsymbol{r})$ in position-space is parity-odd. This means that the definition of standard mean-square axial (charge) radius

$$\langle r_A^2 \rangle \equiv \frac{\int \mathrm{d}^3 r \, r^2 \, J_{5,B}^0(\boldsymbol{r})}{\int \mathrm{d}^3 r \, J_{5,B}^0(\boldsymbol{r})} \tag{37}$$

for a generic spin-$\frac{1}{2}$ system is in fact *not* well-defined. This is different from case for the definition of the mean-square charge radius of the neutron where one can replace $G_E^n(0) = 0$ with $G_E^p(0) = 1$ [1, 147] so as to make the definition well-defined[5], since the nucleon induced (pseudo-)tensor charge $G_T^Z(0)$ in general is not zero [172], see e.g., Eq. (A10).

In the case when $G_T^Z(Q^2) = 0$ by using G-parity invariance of QCD or exact isospin symmetry, the 3D axial density $J_{5,B}^0(\boldsymbol{r})$ vanishes identically for a generic spin-$\frac{1}{2}$ target and thus the axial (charge) radius does not exist [148], contrary to what is usually stated in the literature [19, 20, 58, 59, 104, 173–176] via

$$R_A^2 \equiv -\frac{6}{G_A^Z(0)} \frac{\mathrm{d} G_A^Z(Q^2)}{\mathrm{d} Q^2} \bigg|_{Q^2=0} = \frac{1}{G_A^Z(0)} \left[-\boldsymbol{\nabla}_{\boldsymbol{\Delta}}^2 G_A^Z(\boldsymbol{\Delta}^2) \right] \big|_{\boldsymbol{\Delta}=\boldsymbol{0}}. \tag{38}$$

In conclusion, in either $G_T^Z(Q^2) = 0$ or $G_T^Z(Q^2) \neq 0$ cases, the genuine 3D mean-square axial (charge) radius $\langle r_A^2 \rangle$ is not defined via the slope of the axial FF $G_A^Z(Q^2)$ at $Q^2 = 0$, since the 3D axial charge distribution itself is related to $G_T^Z(Q^2)$ rather than $G_A^Z(Q^2)$.

Before we move forward, there are two key points deserving to be emphasized [148]. The first point is that the relation between a genuine 3D mean-square radius and the slope of the corresponding FF is in general not so obvious and simple, see the examples given in Refs. [148, 167]. One needs to carefully define first the corresponding distribution, and then derive the genuine mean-square radius based on that distribution. The second point is that the concept of identifying a mean-square radius simply via the slope of the corresponding

---

[5] Note also the fact that the BF charge distribution of the neutron is spherically symmetric [142, 147].

FF is in general misleading and incorrect. A typical example is the 3D mean-square axial (charge) radius which is not even related to the axial FF $G_A^Z(Q^2)$, see Eq. (33) and Ref. [148]. On the other hand, it also explicitly reveals the breakdown of Abel transformation in the case of axial charge distributions, see further discussions given in Appendix B.

V. ELASTIC FRAME DISTRIBUTIONS

BF distributions provide us the best proxy for picturing a system in 3D sitting in average at rest around the origin in the Wigner sense, where the spin in the parametrization (1) is defined with respect to the relativistic center of mass. If one is however interested in the internal structure of a moving system, one can employ the so-called elastic frame (EF) distributions introduced in Ref. [139].

Accordingly, the relativistic 2D EF distributions are in general unambiguously defined as [142, 147]

$$
\begin{aligned}
O_{\mathrm{EF}}(\boldsymbol{b}_\perp; P_z) &\equiv \int \mathrm{d}r_z \, \langle \hat{O} \rangle_{\boldsymbol{0},\boldsymbol{P}}^{s's}(\boldsymbol{r}) \\
&= \int \frac{\mathrm{d}^2\Delta_\perp}{(2\pi)^2} \, e^{-i\boldsymbol{\Delta}_\perp \cdot \boldsymbol{b}_\perp} \, \frac{\langle p', s'|\hat{O}(0)|p,s\rangle}{2P^0} \bigg|_{\Delta_z = |\boldsymbol{P}_\perp| = 0},
\end{aligned}
\tag{39}
$$

where the z-axis has been chosen along $\boldsymbol{P} = (\boldsymbol{0}_\perp, P_z)$ without loss of generality, and $\boldsymbol{r} = \boldsymbol{x} - \boldsymbol{R} = (\boldsymbol{b}_\perp, r_z)$ is the position relative to the center $\boldsymbol{R} = \boldsymbol{0}$ of the system. Integrating over the longitudinal coordinate r_z amounts to setting the longitudinal momentum transfer Δ_z to zero, which in turn implies a vanishing energy transfer $\Delta^0 = \boldsymbol{P} \cdot \boldsymbol{\Delta}/P^0 = 0$ and hence time-independent distributions. At $P_z = 0$, the EF distributions (39) coincide with the BF distributions (31) projected onto the transverse plane

$$
O_{\mathrm{EF}}(\boldsymbol{b}_\perp; 0) = \int \mathrm{d}r_z \, O_B(\boldsymbol{r}) = \int \frac{\mathrm{d}^2\Delta_\perp}{(2\pi)^2} \, e^{-i\boldsymbol{\Delta}_\perp \cdot \boldsymbol{b}_\perp} \, \frac{\langle p'_B, s'_B|\hat{O}(0)|p_B, s_B\rangle}{2P_B^0} \bigg|_{\Delta_z = |\boldsymbol{P}| = 0}.
\tag{40}
$$

In the limit $P_z \to \infty$, the EF distributions (39) explicitly reproduce the IMF distributions

$$
O_{\mathrm{IMF}}(\boldsymbol{b}_\perp) \equiv \lim_{P_z \to \infty} O_{\mathrm{EF}}(\boldsymbol{b}_\perp; P_z) = \int \frac{\mathrm{d}^2\Delta_\perp}{(2\pi)^2} \, e^{-i\boldsymbol{\Delta}_\perp \cdot \boldsymbol{b}_\perp} \, \frac{\langle p', s'|\hat{O}(0)|p,s\rangle}{2P^0} \bigg|_{\Delta_z = 0, P_z \to \infty},
\tag{41}
$$

which coincide most of the time with the corresponding LF distributions, up to some trivial

factors [141, 142, 144, 146–149, 177, 178]. EF distribution provides therefore a smooth and physically clear interpolation between the BF and LF distributions.

A.   EF weak-neutral axial-vector four-current distributions

Evaluating directly the matrix elements (1) in the generic EF leads to [148]

$$
\begin{aligned}
\mathcal{A}_{\mathrm{EF}}^{0} &= 2P_z \sigma_z G_A^Z(\boldsymbol{\Delta}_\perp^2) + \frac{P^0}{M}(\boldsymbol{\Delta}_\perp \cdot \boldsymbol{\sigma}_\perp) G_T^Z(\boldsymbol{\Delta}_\perp^2), \\
\mathcal{A}_{\mathrm{EF}}^{z} &= 2P^0 \sigma_z G_A^Z(\boldsymbol{\Delta}_\perp^2) + \frac{P_z}{M}(\boldsymbol{\Delta}_\perp \cdot \boldsymbol{\sigma}_\perp) G_T^Z(\boldsymbol{\Delta}_\perp^2), \\
\boldsymbol{\mathcal{A}}_{\mathrm{EF}}^{\perp} &= 2\sqrt{P^2} \left[\frac{P^0 + M(1+\tau)}{(P^0+M)\sqrt{1+\tau}} \boldsymbol{\sigma}_\perp + \frac{(\boldsymbol{e}_z \times i\boldsymbol{\Delta}_\perp)_\perp}{2M} \frac{P_z}{(P^0+M)\sqrt{1+\tau}} \right] G_A^Z(\boldsymbol{\Delta}_\perp^2) \\
&\quad - \frac{\boldsymbol{\Delta}_\perp(\boldsymbol{\Delta}_\perp \cdot \boldsymbol{\sigma}_\perp)}{2} \left[\frac{G_A^Z(\boldsymbol{\Delta}_\perp^2)}{P^0+M} + \frac{G_P^Z(\boldsymbol{\Delta}_\perp^2)}{M} \right],
\end{aligned}
\tag{42}
$$

where $\mathcal{A}_{\mathrm{EF}}^{\mu} \equiv \langle p', s' | \hat{j}_5^\mu(0) | p, s \rangle$, $p' = (P^0, \boldsymbol{\Delta}_\perp/2, P_z)$, $p = (P^0, -\boldsymbol{\Delta}_\perp/2, P_z)$, $Q^2 = \boldsymbol{\Delta}_\perp^2$, and $P^0 = \sqrt{M^2(1+\tau) + P_z^2}$.

Poincaré symmetry can also be employed to determine how the matrix elements of the axial-vector four-current operator in different Lorentz frames are related to each other. One can write in general [130, 131]

$$
\langle p', s' | \hat{j}_5^\mu(0) | p, s \rangle = \sum_{s_B', s_B} D_{s's_B'}^{\dagger(j)}(p_B', \Lambda) D_{s_B s}^{(j)}(p_B, \Lambda) \, \Lambda^\mu{}_\nu \, \langle p_B', s_B' | \hat{j}_5^\nu(0) | p_B, s_B \rangle,
\tag{43}
$$

where $\langle p_B', s_B' | \hat{j}_5^\nu(0) | p_B, s_B \rangle$ represents the BF matrix elements, Λ is the rotationless Lorentz boost matrix from the BF to a generic Lorentz frame, and $D^{(j)}$ is the Wigner rotation matrix for a generic spin-j system. Alternatively, one can *analytically* reproduce above EF amplitudes (42) by applying the covariant Lorentz transformation (43) on the BF amplitudes (32) at $\Delta_z = 0$, where the Wigner rotation matrix $D^{(1/2)}$ is explicitly given by [146, 147]

$$
\begin{aligned}
D^{(1/2)}(p_B, \Lambda) &= D^{\dagger(1/2)}(p_B', \Lambda) \\
&= \begin{pmatrix} \cos\frac{\theta}{2} & -e^{-i\phi_\Delta} \sin\frac{\theta}{2} \\ e^{i\phi_\Delta} \sin\frac{\theta}{2} & \cos\frac{\theta}{2} \end{pmatrix}
\end{aligned}
\tag{44}
$$

with $\boldsymbol{\Delta} = Q(\cos\phi_\Delta, \sin\phi_\Delta, 0)$ and θ being the *Wigner rotation angle*. We indeed explicitly

reproduce our previous results in electromagnetic four-current, polarization-magnetization tensor and axial-vector four-current (without the second-class current contribution) cases for the Wigner angular conditions: [144, 146–148]

$$\cos\theta = \frac{P^0 + M(1+\tau)}{(P^0 + M)\sqrt{1+\tau}},$$

$$\sin\theta = -\frac{\sqrt{\tau}P_z}{(P^0 + M)\sqrt{1+\tau}}. \tag{45}$$

As a result, the EF amplitudes (42) can be equivalently rewritten as

$$\mathcal{A}_{\mathrm{EF}}^0 = 2M\gamma\sqrt{1+\tau}\left[\beta\sigma_z G_A^Z(\boldsymbol{\Delta}_\perp^2) + \frac{(\boldsymbol{\sigma}_\perp\cdot\boldsymbol{\Delta}_\perp)}{2M}G_T^Z(\boldsymbol{\Delta}_\perp^2)\right],$$

$$\mathcal{A}_{\mathrm{EF}}^z = 2M\gamma\sqrt{1+\tau}\left[\sigma_z G_A^Z(\boldsymbol{\Delta}_\perp^2) + \beta\frac{(\boldsymbol{\sigma}_\perp\cdot\boldsymbol{\Delta}_\perp)}{2M}G_T^Z(\boldsymbol{\Delta}_\perp^2)\right],$$

$$\mathcal{A}_{\mathrm{EF}}^\perp = 2M\sqrt{1+\tau}\left\{\boldsymbol{\sigma}_\perp + \frac{(i\boldsymbol{\Delta}_\perp\times\boldsymbol{e}_z)_\perp}{|\boldsymbol{\Delta}_\perp|}\left[\sin\theta + \frac{(i\boldsymbol{\Delta}_\perp\times\boldsymbol{\sigma})_z}{|\boldsymbol{\Delta}_\perp|}(\cos\theta - 1)\right]\right\}G_A^Z(\boldsymbol{\Delta}_\perp^2) \tag{46}$$

$$- \frac{\boldsymbol{\Delta}_\perp(\boldsymbol{\Delta}_\perp\cdot\boldsymbol{\sigma}_\perp)}{2M}\left[\frac{G_A^Z(\boldsymbol{\Delta}_\perp^2)}{1+\sqrt{1+\tau}} + G_P^Z(\boldsymbol{\Delta}_\perp^2)\right],$$

with [146, 147]

$$\gamma = \gamma(Q) = \frac{P^0}{M\sqrt{1+\tau}} = \frac{P^0}{\sqrt{P^2}}, \qquad \beta = \beta(Q) = \frac{P_z}{P^0}, \tag{47}$$

where $\mathcal{A}_{\mathrm{EF}}^\perp$ can also be alternatively but equivalently rewritten as [148]

$$\mathcal{A}_{\mathrm{EF}}^\perp = 2\sqrt{P^2}\left[\boldsymbol{\sigma}_\perp\cos\theta - \frac{(\boldsymbol{e}_z\times i\boldsymbol{\Delta}_\perp)_\perp}{2M\sqrt{\tau}}\sin\theta\right]G_A^Z(\boldsymbol{\Delta}_\perp^2)$$

$$- \frac{\boldsymbol{\Delta}_\perp(\boldsymbol{\Delta}_\perp\cdot\boldsymbol{\sigma}_\perp)}{2}\left[\frac{G_A^Z(\boldsymbol{\Delta}_\perp^2)}{P^0 + M} + \frac{G_P^Z(\boldsymbol{\Delta}_\perp^2)}{M}\right]. \tag{48}$$

We emphasize that the Wigner rotation will in general distort the original distributions in the frame before the Lorentz boost, resulting physical distortions in another frame after the Lorentz boost (43), see e.g., the Q-dependent $\sin\theta$ and $\cos\theta$ factors in terms of the Wigner rotation angle θ in $\mathcal{A}_{\mathrm{EF}}^\perp$.

Applying the general definition (39) to the axial-vector four-current operator and inserting the EF amplitudes from Eqs. (42) or (46,48), we obtain the following relativistic EF weak-
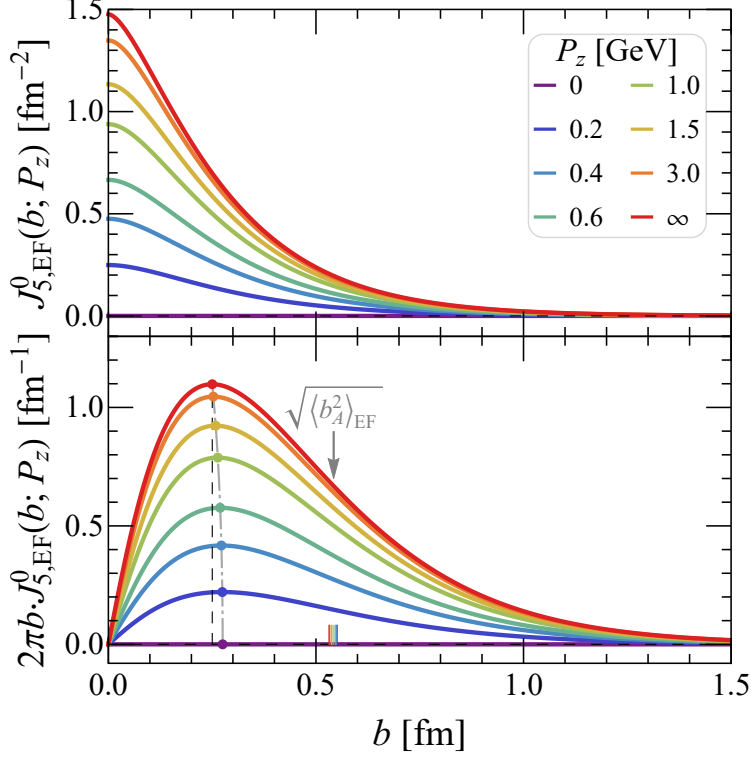
FIG. 4. Frame-dependence of EF weak-neutral axial charge distributions $J_{5,\text{EF}}^0(b; P_z)$ (upper panel) and $2\pi b \cdot J_{5,\text{EF}}^0(b; P_z)$ (lower panel) as a function $b = |\boldsymbol{b}_\perp|$ inside a longitudinally polarized (i.e. $\hat{\boldsymbol{s}} = \boldsymbol{e}_z$) proton, using proton's weak-neutral axial FF $G_A^Z(Q^2)$ given in Appendix A. Maxima of $2\pi b \cdot J_{5,\text{EF}}^0$ are indicated by the gray dot-dashed curve, and the corresponding root-mean-square transverse axial (charge) radii $\sqrt{\langle b_A^2 \rangle_{\text{EF}}}$ of $J_{5,\text{EF}}^0$ from Eq. (51) are also marked in the lower panel.

neutral axial-vector four-current distributions:

$$
\begin{aligned}
J_{5,\text{EF}}^0(\boldsymbol{b}_\perp; P_z) &= \int \frac{\mathrm{d}^2\Delta_\perp}{(2\pi)^2} e^{-i\boldsymbol{\Delta}_\perp \cdot \boldsymbol{b}_\perp} \left[\left(\frac{P_z}{P^0}\right) \sigma_z G_A^Z(\boldsymbol{\Delta}_\perp^2) + \frac{\boldsymbol{\Delta}_\perp \cdot \boldsymbol{\sigma}_\perp}{2M} G_T^Z(\boldsymbol{\Delta}_\perp^2) \right], \\
J_{5,\text{EF}}^z(\boldsymbol{b}_\perp; P_z) &= \int \frac{\mathrm{d}^2\Delta_\perp}{(2\pi)^2} e^{-i\boldsymbol{\Delta}_\perp \cdot \boldsymbol{b}_\perp} \left[\sigma_z G_A^Z(\boldsymbol{\Delta}_\perp^2) + \left(\frac{P_z}{P^0}\right) \frac{\boldsymbol{\Delta}_\perp \cdot \boldsymbol{\sigma}_\perp}{2M} G_T^Z(\boldsymbol{\Delta}_\perp^2) \right], \\
\boldsymbol{J}_{5,\text{EF}}^\perp(\boldsymbol{b}_\perp; P_z) &= \int \frac{\mathrm{d}^2\Delta_\perp}{(2\pi)^2} e^{-i\boldsymbol{\Delta}_\perp \cdot \boldsymbol{b}_\perp} \left\{ -\frac{\boldsymbol{\Delta}_\perp(\boldsymbol{\Delta}_\perp \cdot \boldsymbol{\sigma}_\perp)}{4P^0} \left[\frac{G_A^Z(\boldsymbol{\Delta}_\perp^2)}{P^0 + M} + \frac{G_P^Z(\boldsymbol{\Delta}_\perp^2)}{M} \right] \right. \\
&\quad \left. + \frac{\sqrt{P^2}}{P^0} \left[\cos\theta\, \boldsymbol{\sigma}_\perp - \frac{(\boldsymbol{e}_z \times i\boldsymbol{\Delta}_\perp)_\perp}{2M\sqrt{\tau}} \sin\theta \right] G_A^Z(\boldsymbol{\Delta}_\perp^2) \right\}.
\end{aligned}
\tag{49}
$$

In the case $G_T^Z(\boldsymbol{\Delta}_\perp^2) = 0$, we do explicitly reproduce the EF axial-vector four-current distributions given in Ref. [148]. In Fig. 4, we illustrate the EF axial charge distributions $J_{5,\text{EF}}^0(b; P_z)$ and $2\pi b \cdot J_{5,\text{EF}}^0(b; P_z)$ as a function of $b = |\boldsymbol{b}_\perp|$ inside a longitudinally polarized (i.e. $\hat{\boldsymbol{s}} = \boldsymbol{e}_z$) proton at different P_z, using proton's weak-neutral axial FF $G_A^Z(Q^2)$
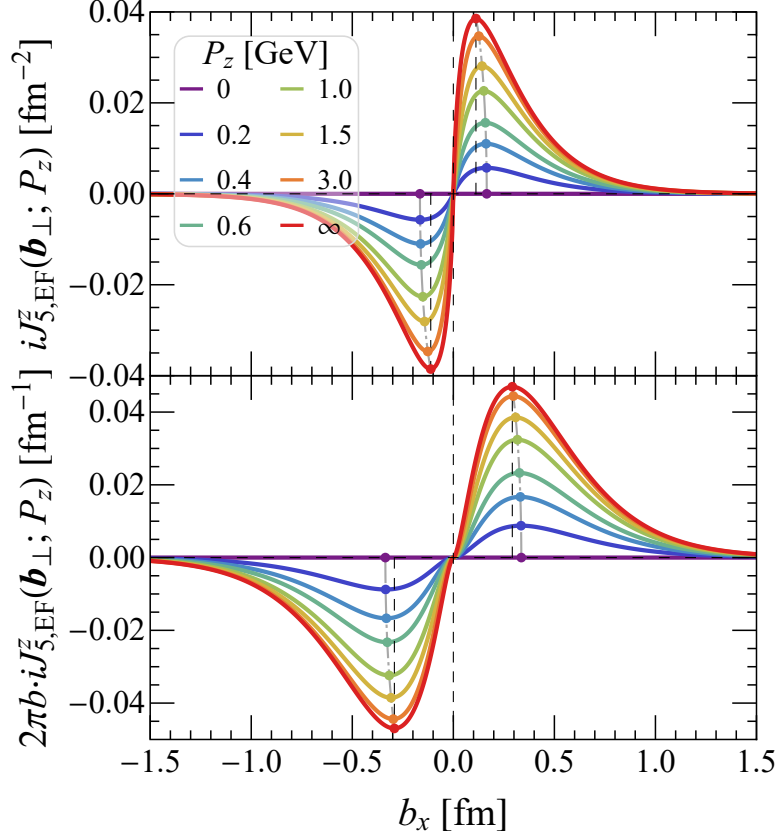
FIG. 5. Frame-dependence of EF weak-neutral longitudinal axial-vector current distributions $iJ_{5,\mathrm{EF}}^z(\boldsymbol{b}_\perp; P_z)$ (upper panel) and $2\pi b \cdot iJ_{5,\mathrm{EF}}^z(\boldsymbol{b}_\perp; P_z)$ (lower panel) along the x-axis inside a transversely polarized (i.e. $\hat{\boldsymbol{s}} = \boldsymbol{e}_x$) proton, using proton's weak-neutral induced (pseudo-)tensor FF $G_T^Z(Q^2)$ given in Appendix A. The maxima (minima) are indicated by the gray dot-dashed curves.

given in Appendix A. According to Eq. (49), it is clear that $J_{5,\mathrm{EF}}^0(\boldsymbol{b}_\perp; \infty) = J_{5,\mathrm{EF}}^z(\boldsymbol{b}_\perp; \infty)$, which is quite reminiscent of the cases for the electromagnetic four-current [146] and polarization-magnetization [147] distributions in the IMF limit $P_z \to \infty$. In Fig. 5, we illustrate the parity-odd longitudinal axial-vector current distributions $iJ_{5,\mathrm{EF}}^z(\boldsymbol{b}_\perp; P_z)$ and $2\pi b \cdot iJ_{5,\mathrm{EF}}^z(\boldsymbol{b}_\perp; P_z)$ along the x-axis at different P_z inside a transversely polarized proton, using proton's weak-neutral induced (pseudo-)tensor FF $G_T^Z(Q^2)$ given in Appendix A.

Similarly to what we have mentioned in the BF case (33), we do observe that the transverse EF axial-vector current $\boldsymbol{J}_{5,\mathrm{EF}}^\perp$ is indeed independent of $G_T^Z(Q^2)$, since the transverse part of the BF axial-vector four-current amplitudes (32) does not get mixed under longitudinal Lorentz boosts (33). In Fig. 6, we illustrate the transverse EF weak-neutral axial-vector current distribution $\boldsymbol{J}_{5,\mathrm{EF}}^\perp(\boldsymbol{b}_\perp; P_z)$ in the transverse plane inside a transversely polarized (i.e. $\hat{\boldsymbol{s}} = \boldsymbol{e}_x$) proton at $P_z = 2$ GeV, using proton's weak-neutral axial-vector FFs $G_A^Z(Q^2)$ and
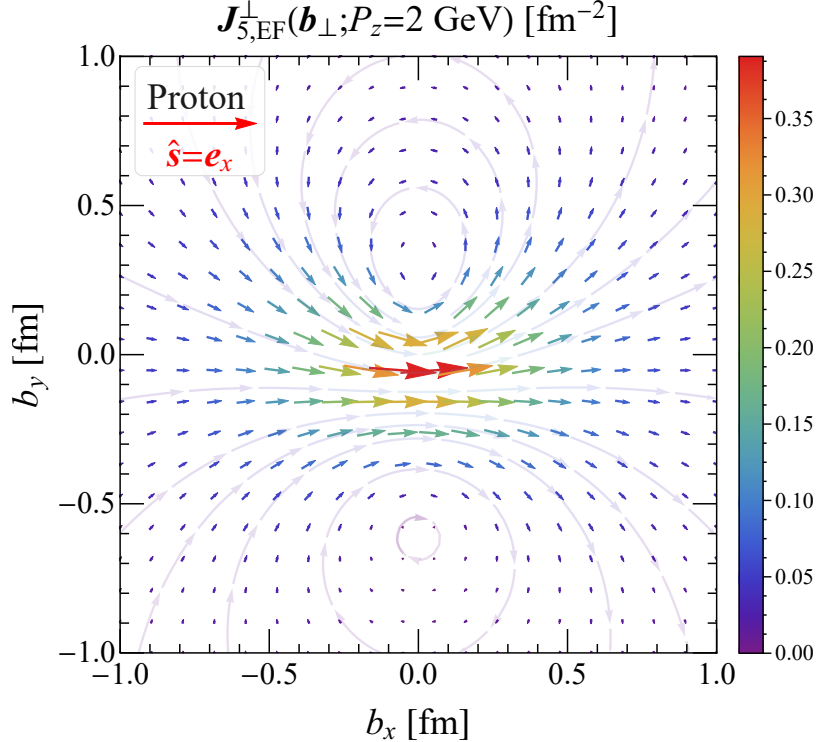
FIG. 6. The transverse EF weak-neutral axial-vector current distribution $\boldsymbol{J}_{5,\mathrm{EF}}^{\perp}(\boldsymbol{b}_{\perp}; P_z)$ in the transverse plane inside a transversely polarized (i.e. $\hat{\boldsymbol{s}} = \boldsymbol{e}_x$) proton at $P_z = 2$ GeV, using proton's weak-neutral axial-vector FFs $G_A^Z(Q^2)$ and $G_P^Z(Q^2)$ given in Appendix A.

$G_P^Z(Q^2)$ given in Appendix A. We observe that the EF distribution $\boldsymbol{J}_{5,\mathrm{EF}}^{\perp}$ at $P_z = 2$ GeV, compared with the BF one $\boldsymbol{J}_{5,B}^{\perp}$ at $P_z = 0$ in Fig. 3, is no longer mirror symmetric with respect to the x-axis but is still mirror antisymmetric with respect to the y-axis in the transverse plane, as long as P_z is finite and nonvanishing. The key reason is that on top of the monopole and quadrupole contributions, $\boldsymbol{J}_{5,\mathrm{EF}}^{\perp}$ at finite P_z also contains a dipole contribution, which explicitly breaks the up-down mirror symmetry (with respect to the x-axis) but still preserves the left-right mirror antisymmetry (with respect to the y-axis) in the transverse plane for a transversely polarized spin-$\frac{1}{2}$ system.

Furthermore, owing to the mixing of temporal and longitudinal components of the axial-vector four-current under a longitudinal Lorentz boost, we also observe that as long as $|P_z| > 0$ the generic EF distributions $J_{5,\mathrm{EF}}^0$ and $J_{5,\mathrm{EF}}^z$ begin to depend on $G_A^Z(Q^2)$ and $G_T^Z(Q^2)$ respectively, in comparison with those BF ones (33). Moreover, we note that both $J_{5,\mathrm{EF}}^0$ and $J_{5,\mathrm{EF}}^z$ in the generic EF are free from the Wigner rotation (43) while $\boldsymbol{J}_{5,\mathrm{EF}}^{\perp}$ suffers from that (see, e.g., the $\cos\theta$ and $\sin\theta$ factors in $\boldsymbol{J}_{5,\mathrm{EF}}^{\perp}$), since the Wigner rotation (43) mixes $(\boldsymbol{\sigma}_{\perp})_{s's}$ while leaves $(\sigma_z)_{s's}$ and $(\boldsymbol{\Delta}_{\perp} \cdot \boldsymbol{\sigma}_{\perp})_{s's}$ unchanged [147].

B. EF mean-square transverse radii

Following Refs. [147, 148], we are now ready to rederive mean-square transverse axial and spin radii for a general spin-$\frac{1}{2}$ hadron in the generic EF. In the 2D case, the mean-square transverse radius of a 2D spatial distribution $O(\boldsymbol{b}_\perp; \mathcal{K})$ is in general given by

$$\langle b_O^2 \rangle(\mathcal{K}) \equiv \frac{\int \mathrm{d}^2 b_\perp\, b^2\, O(\boldsymbol{b}_\perp; \mathcal{K})}{\int \mathrm{d}^2 b_\perp\, O(\boldsymbol{b}_\perp; \mathcal{K})}, \tag{50}$$

where $\mathcal{K}$ denotes a set of external momentum information, e.g., $\mathcal{K} = P_z$ in the 2D EF case [see e.g. Eq. (49)] and $\mathcal{K} = P^+$ in the LF case [see e.g. Eq. (61) in the following Sec. VI].

Applying this general definition (50) to the 2D EF axial charge $J_{5,\mathrm{EF}}^0(\boldsymbol{b}_\perp; P_z)$ and longitudinal spin $S_{\mathrm{EF}}^z(\boldsymbol{b}_\perp; P_z) = J_{5,\mathrm{EF}}^z(\boldsymbol{b}_\perp; P_z)/2$ distributions (49), we find

$$\begin{aligned}
\langle b_A^2 \rangle_{\mathrm{EF}}(P_z) &\equiv \frac{\int \mathrm{d}^2 b_\perp\, b^2\, J_{5,\mathrm{EF}}^0(\boldsymbol{b}_\perp; P_z)}{\int \mathrm{d}^2 b_\perp\, J_{5,\mathrm{EF}}^0(\boldsymbol{b}_\perp; P_z)} = \frac{1}{2E_P^2} + \frac{2}{3}R_A^2, \\
\langle b_{\mathrm{spin},L}^2 \rangle_{\mathrm{EF}}(P_z) &\equiv \frac{\int \mathrm{d}^2 b_\perp\, b^2\, S_{\mathrm{EF}}^z(\boldsymbol{b}_\perp; P_z)}{\int \mathrm{d}^2 b_\perp\, S_{\mathrm{EF}}^z(\boldsymbol{b}_\perp; P_z)} = \frac{2}{3}R_A^2,
\end{aligned} \tag{51}$$

which explicitly coincide with the results given in Ref. [148], with $E_P = \sqrt{M^2 + P_z^2}$ and R_A^2 given in Eq. (38). Besides, since $\boldsymbol{J}_{5,\mathrm{EF}}^\perp$ in Eq. (49) assumes exactly the same expression as in Ref. [148], we expect the same result for the mean-square transverse spin radius [148]

$$\langle b_{\mathrm{spin},T}^2 \rangle_{\mathrm{EF}}(P_z) = \frac{2}{3}R_A^2 + \frac{1}{2M^2}\frac{G_P^Z(0)}{G_A^Z(0)} + \frac{1}{2E_P^2} - \frac{1}{2M(E_P + M)}. \tag{52}$$

In Fig. 7, we show the mean-square transverse spin radius $\langle b_{\mathrm{spin},T}^2 \rangle_{\mathrm{EF}}(P_z)$ as a function of P_z for the proton in the generic EF, where $R_A^2 = 12/(M_A^Z)^2 \approx (0.6510\,\mathrm{fm})^2$ and $G_P^Z(0)/G_A^Z(0) = (2M_p/M_\pi)^2 \approx 180.772$ by using proton's weak-neutral axial-vector FFs $G_A^Z(Q^2)$ and $G_P^Z(Q^2)$ given in Appendix A. In particular, we find that the minimum of $\langle b_{\mathrm{spin},T}^2 \rangle_{\mathrm{EF}}(P_z)$ is located at $P_z \simeq 3.2132\, M_p \approx 3.0149\,\mathrm{GeV}$, while the maximum of $\langle b_{\mathrm{spin},T}^2 \rangle_{\mathrm{EF}}(P_z)$ is located at $P_z = 0$. At IMF limit $P_z \to \infty$, the value of $\langle b_{\mathrm{spin},T}^2 \rangle_{\mathrm{EF}}(\infty)$ is entirely contributed by the first two terms (52), lying in between $\langle b_{\mathrm{spin},T}^2 \rangle_{\mathrm{EF}}(0)$ and $\langle b_{\mathrm{spin},T}^2 \rangle_{\mathrm{EF}}(P_z \simeq 3.2132\, M_p)$.

From Eqs. (51) and (52), we conclude that although we explicitly include the second-class current contribution associated with $G_T^Z(Q^2)$ in the full matrix elements (1) and $G_T^Z(Q^2)$ indeed enters both $J_{5,\mathrm{EF}}^0$ and $J_{5,\mathrm{EF}}^z$ in Eq. (49), this second-class current contribution does
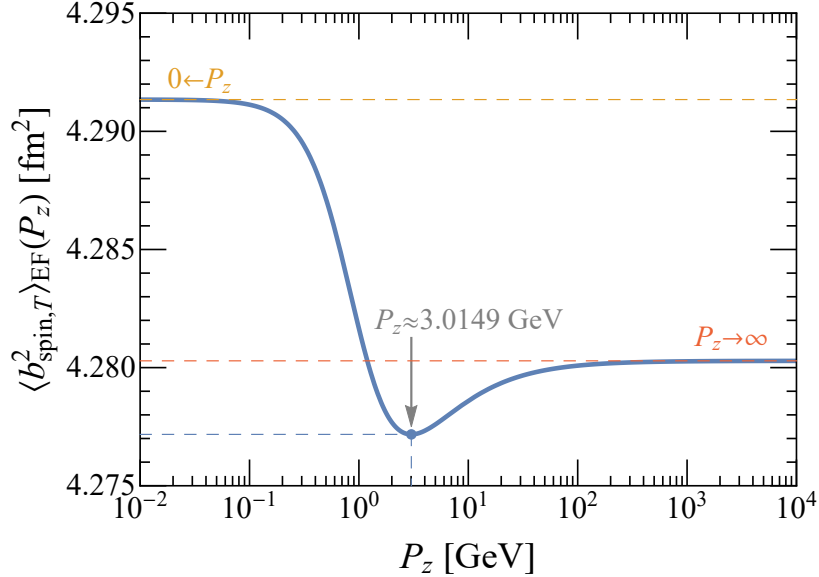
FIG. 7. The mean-square transverse spin radius $\langle b_{\mathrm{spin},T}^2\rangle_{\mathrm{EF}}(P_z)$ of the proton from Eq. (52) as a function of P_z, using proton's weak-neutral axial-vector FFs $G_A^Z(0)$ and $G_P^Z(0)$ given in Appendix A. The minimum of $\langle b_{\mathrm{spin},T}^2\rangle_{\mathrm{EF}}(P_z)$ is located at $P_z \simeq 3.2132\, M_p \approx 3.0149$ GeV.

not contribute in fact to the mean-square transverse axial and spin radii in the generic EF.

VI. LIGHT-FRONT DISTRIBUTIONS

For completeness, we finally study the relativistic axial-vector four-current distributions including the second-class current contribution (1) by using the LF formalism [115], where LF distributions in some cases can be interpreted as *strict* probabilistic densities [118–128], since the symmetry group associated with the transverse LF plane is the Galilean subgroup singled out from the Lorentz group [116, 117].

In the LF formalism [115], a generic four-vector a^μ is denoted as $a^\mu = [a^+, a^-, \boldsymbol{a}_\perp]$ with $a^\pm \equiv (a^0 \pm a^3)/\sqrt{2}$. As a result, scalar products read $p \cdot x = p^\mu x_\mu = p^+ x^- + p^- x^+ - \boldsymbol{p}_\perp \cdot \boldsymbol{x}_\perp$, and the constrained LF momentum component p^- is then given by $p^- = (\boldsymbol{p}_\perp^2 + M^2)/(2p^+)$ by using the on-mass-shell condition $p^2 = 2p^+p^- - \boldsymbol{p}_\perp^2 = M^2$.

It is possible to define x^+-independent LF distributions [118, 125, 139] in the so-called symmetric LF frame specified by the conditions[6]: $\boldsymbol{P}_\perp = \boldsymbol{0}_\perp$ and $\Delta^+ = 0$, which ensure that the LF energy transfer $\Delta^- = (\boldsymbol{P}_\perp \cdot \boldsymbol{\Delta}_\perp - P^-\Delta^+)/P^+$ vanishes automatically. Similar to

---

[6] One can relax the condition $\boldsymbol{P}_\perp = \boldsymbol{0}_\perp$, provided that LF distributions are restricted to $x^+ = 0$ [179, 180].

Eq. (39), probabilistic LF distributions are in general defined as

$$O_{\mathrm{LF}}(\boldsymbol{b}_\perp; P^+) \equiv \int \frac{\mathrm{d}^2\Delta_\perp}{(2\pi)^2}\, e^{-i\boldsymbol{\Delta}_\perp \cdot \boldsymbol{b}_\perp}\, \frac{{}_{\mathrm{LF}}\langle p', \lambda' | \hat{O}(0) | p, \lambda \rangle_{\mathrm{LF}}}{2P^+}\bigg|_{\Delta^+ = |\boldsymbol{P}_\perp| = 0}, \tag{53}$$

where P^+ is treated as an independent variable in LF formalism, and LF helicity states $|p, \lambda\rangle_{\mathrm{LF}}$ are covariantly normalized as

$$_{\mathrm{LF}}\langle p', \lambda' | p, \lambda \rangle_{\mathrm{LF}} = 2p^+(2\pi)^3\delta(p'^+ - p^+)\delta^{(2)}(\boldsymbol{p}'_\perp - \boldsymbol{p}_\perp)\delta_{\lambda'\lambda}, \tag{54}$$

and can be related to the generic canonical spin states $|p, s\rangle$ via the Melosh rotation [132]

$$|p, \lambda\rangle_{\mathrm{LF}} = \sum_s \frac{|p, s\rangle\langle p, s|}{\langle p, s | p, s \rangle}|p, \lambda\rangle_{\mathrm{LF}} = \sum_s |p, s\rangle \mathcal{M}^{(j)}_{s\lambda}(p), \qquad \mathcal{M}^{(j)}_{s\lambda}(p) \equiv \frac{\langle p, s | p, \lambda \rangle_{\mathrm{LF}}}{\langle p, s | p, s \rangle}, \tag{55}$$

where $\mathcal{M}^{(j)}_{s\lambda}(p)$ denotes the unitary matrix elements of the Melosh rotation for a spin-j system. We note that some of the unusual distortions appearing in LF distributions are relativistic artefacts caused by Melosh rotations [133, 142, 144, 146, 147], since $\mathcal{M}^{(j)}(p)$ in general is not an identity matrix.

In the spin-$\frac{1}{2}$ case that we mainly focus on in this work, the generic 2×2 unitary Melosh rotation matrix $\mathcal{M}^{(1/2)}$ is explicitly given by [133, 146, 147]

$$\mathcal{M}^{(1/2)}(p) = \begin{pmatrix} \cos\frac{\theta_M}{2} & -e^{-i\phi_p}\sin\frac{\theta_M}{2} \\ e^{i\phi_p}\sin\frac{\theta_M}{2} & \cos\frac{\theta_M}{2} \end{pmatrix} = \frac{1}{\sqrt{\mathcal{N}_p}}\begin{pmatrix} p^0 + p_z + M, & -(p_x - ip_y) \\ p_x + ip_y, & p^0 + p_z + M \end{pmatrix}, \tag{56}$$

with

$$\begin{aligned} \cos\theta_M &= \frac{(p^0 + p_z + M)^2 - |\boldsymbol{p}_\perp|^2}{\mathcal{N}_p}, \\ \sin\theta_M &= -\frac{2(p^0 + p_z + M)|\boldsymbol{p}_\perp|}{\mathcal{N}_p}, \end{aligned} \tag{57}$$

where $\mathcal{N}_p \equiv 2(p^0 + p_z)(p^0 + M) = (p^0 + p_z + m)^2 + \boldsymbol{p}_\perp^2$, $\boldsymbol{p}_\perp = |\boldsymbol{p}_\perp|(\cos\phi_p, \sin\phi_p)$, and θ_M is the *Melosh rotation angle*. It is easy to verify that $\cos^2\theta_M + \sin^2\theta_M = 1$ is indeed automatically guaranteed.

In Fig. 8, we illustrate the Melosh rotation angle θ_M and $\cos\theta_M$ for the proton in the generic EF as a function of the average momentum $P_z = p_z$ and the momentum transfer
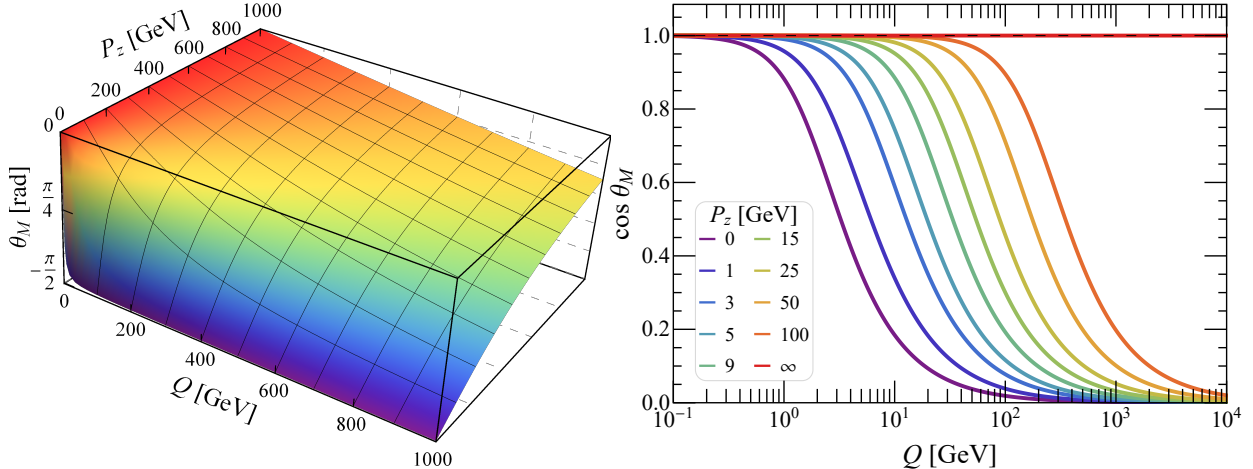
FIG. 8. Melosh rotation angle θ_M (left panel) and $\cos\theta_M$ (right panel) for the proton in the generic EF as a function of the average momentum P_z and the momentum transfer magnitude $Q = |\mathbf{\Delta}_\perp|$.

magnitude $Q = |\mathbf{\Delta}_\perp| = 2|\mathbf{p}_\perp|$. In particular when $P_z = 0$, we have

$$\lim_{P_z \to 0} \cos\theta_M = \frac{1}{\sqrt{1+\tau}}, \qquad \lim_{P_z \to 0} \sin\theta_M = -\frac{\sqrt{\tau}}{\sqrt{1+\tau}}, \tag{58}$$

which are well consistent with what we have found in Ref. [146]. When $P_z \to \infty$, $\theta_M = 0$ and $\mathcal{M}^{(1/2)}(p)$ will be an identity matrix. We also observe that as long as $Q \neq 0$ and $|P_z| \neq \infty$, $\mathcal{M}^{(1/2)}(p)$ will not be an identity matrix. In most of the LF distributions in the literature, see e.g. Refs. [118–126], $Q = 2|\mathbf{p}_\perp| \neq 0$ is evident since people wish to present the 2D LF distributions on the transverse (or impact parameter) plane.

One may argue that the as long as the limit $P_z \to \infty$ is taken, LF amplitudes should be completely free from relativistic artefacts caused by Melosh rotations, since the LF amplitudes can be explicitly obtained via the IMF limit $P_z \to \infty$ of the EF amplitudes [146–148]. This is not true, since when we take the IMF limit $P_z \to \infty$ of EF amplitudes, see e.g. Sec. VI B, we keep both $(P^0 + P_z)/\sqrt{2} \equiv P^+$ and $(P^0 - P_z)/\sqrt{2} \equiv P^-$ fixed. When $P^+ \neq \infty$ and $P^- \neq 0$, relativistic artefacts caused by Melosh rotations may have been inherited partially in the LF amplitudes, see e.g. $\mathcal{A}_{\text{LF}}^-$ in Eq. (60). Typically, when a well-defined LF distribution is completely independent of both P^+ and P^-, e.g. the LF electric charge distribution J_{LF}^+ [147] and axial charge distribution $J_{5,\text{LF}}^+$ (61) of the nucleon, it should be free from relativistic artefacts caused by Melosh rotations [133, 142, 144, 146, 147]. From the Melosh rotation perspective, this also explains the reason why the LF components $\hat{j}^+$

and $\hat{j}^-$ are usually regarded as the "good" and "bad" components in the literature [146], respectively. In this sense, we believe that the pictures provided by those LF densities that depend explicitly on P^+ or P^- can *not* be considered as realistic representations of the system (on the average) at rest [147].

Another substantial part of distortions appearing in LF distributions are physically induced by Wigner rotations [146]. According to the generic Lorentz transformation [130, 131] of matrix elements from one frame Σ to another Lorentz frame Σ' based on Poincaré symmetry, the Wigner rotation will in general distort the distributions (in the Σ frame) during the Lorentz boost, resulting therefore physical distortions in the Σ' frame. Since one can always explicitly reproduce the LF amplitudes based on the proper IMF limit of canonical EF amplitudes [146–148] where the Wigner rotation has already played an important role, see e.g. Sec. VI B, we conclude that some of the distortions appearing in LF distributions are natural relativistic consequences of physical Wigner rotations rather than artefacts owing to the change of Dirac spinors from canonical spin basis to LF helicity basis (55).

A. LF weak-neutral axial-vector four-current distributions

By analogy with Eq. (1), matrix elements of the axial-vector four-current operator in terms of LF helicity states $|p, \lambda\rangle_{\mathrm{LF}}$ for a general spin-$\frac{1}{2}$ system are parametrized as [148]

$$_{\mathrm{LF}}\langle p', \lambda'|\hat{j}_5^\mu(0)|p, \lambda\rangle_{\mathrm{LF}} = \bar{u}_{\mathrm{LF}}(p', \lambda') \left[\gamma^\mu G_A^Z + \frac{\Delta^\mu}{2M} G_P^Z + \frac{i\sigma^{\mu\nu}\Delta_\nu}{2M} G_T^Z \right] \gamma^5 u_{\mathrm{LF}}(p, \lambda), \qquad (59)$$

where $u_{\mathrm{LF}}(p, \lambda)$ denotes the LF helicity Dirac spinor, and the explicit Q^2-dependence of these axial-vector FFs $G_A^Z(Q^2)$, $G_P^Z(Q^2)$, and $G_T^Z(Q^2)$ for clarity is omitted.

Evaluating directly the matrix elements (59) in the symmetric LF frame leads to [148]

$$\mathcal{A}_{\mathrm{LF}}^+ = 2P^+(\sigma_z)_{\lambda'\lambda} G_A^Z(\mathbf{\Delta}_\perp^2) + \frac{P^+}{M}(\mathbf{\Delta}_\perp \cdot \boldsymbol{\sigma}_\perp)_{\lambda'\lambda} G_T^Z(\mathbf{\Delta}_\perp^2),$$

$$\mathcal{A}_{\mathrm{LF}}^- = -2P^-(\sigma_z)_{\lambda'\lambda} G_A^Z(\mathbf{\Delta}_\perp^2) + \frac{P^-}{M}(\mathbf{\Delta}_\perp \cdot \boldsymbol{\sigma}_\perp)_{\lambda'\lambda} G_T^Z(\mathbf{\Delta}_\perp^2), \qquad (60)$$

$$\mathcal{A}_{\mathrm{EF}}^\perp = [2M(\boldsymbol{\sigma}_\perp)_{\lambda'\lambda} + (\boldsymbol{e}_z \times i\mathbf{\Delta}_\perp)_\perp \delta_{\lambda'\lambda}] G_A^Z(\mathbf{\Delta}_\perp^2) - \frac{\mathbf{\Delta}_\perp (\mathbf{\Delta}_\perp \cdot \boldsymbol{\sigma}_\perp)_{\lambda'\lambda}}{2M} G_P^Z(\mathbf{\Delta}_\perp^2),$$

where $\mathcal{A}_{\mathrm{LF}}^\mu \equiv {}_{\mathrm{LF}}\langle p', \lambda'|\hat{j}_5^\mu(0)|p, \lambda\rangle_{\mathrm{LF}}$, $p' = [P^+, P^-, \mathbf{\Delta}_\perp/2]$, $p = [P^+, P^-, -\mathbf{\Delta}_\perp/2]$, $Q^2 = \mathbf{\Delta}_\perp^2$,

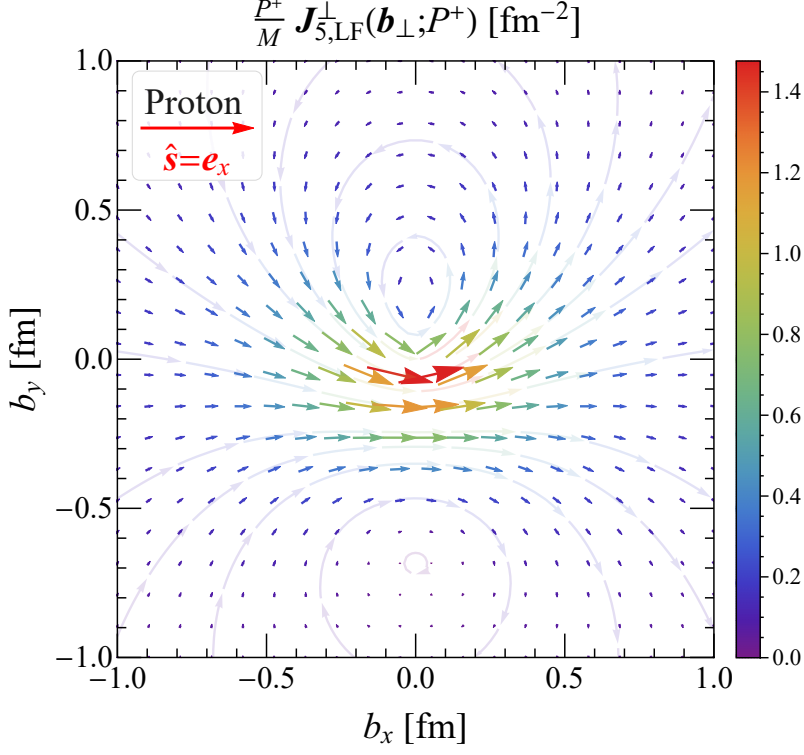$$\frac{P^+}{M}\, \boldsymbol{J}^\perp_{5,\text{LF}}(\boldsymbol{b}_\perp; P^+)\ [\text{fm}^{-2}]$$

FIG. 9. The (scaled) transverse LF weak-neutral axial-vector current distribution $\frac{P^+}{M}\boldsymbol{J}^\perp_{5,\text{LF}}(\boldsymbol{b}_\perp; P^+)$ in the transverse plane inside a transversely polarized (i.e. $\hat{\boldsymbol{s}} = \boldsymbol{e}_x$) proton, using proton's weak-neutral axial-vector FFs $G^Z_A(Q^2)$ and $G^Z_P(Q^2)$ given in Appendix A.

$P^2 = M^2(1 + \tau)$ and $P^- = M^2(1 + \tau)/(2P^+)$. Applying the general definition (53) to the axial-vector four-current operator and inserting the EF amplitudes (60), we obtain the following LF weak-neutral axial-vector four-current distributions [148, 181]:

$$
\begin{aligned}
J^+_{5,\text{LF}}(\boldsymbol{b}_\perp; P^+) &= \int \frac{\mathrm{d}^2\boldsymbol{\Delta}_\perp}{(2\pi)^2}\, e^{-i\boldsymbol{\Delta}_\perp \cdot \boldsymbol{b}_\perp}\left[(\sigma_z)_{\lambda'\lambda} G^Z_A(\boldsymbol{\Delta}^2_\perp) + \frac{(\boldsymbol{\Delta}_\perp \cdot \boldsymbol{\sigma}_\perp)_{\lambda'\lambda}}{2M} G^Z_T(\boldsymbol{\Delta}^2_\perp)\right], \\
J^-_{5,\text{LF}}(\boldsymbol{b}_\perp; P^+) &= \int \frac{\mathrm{d}^2\boldsymbol{\Delta}_\perp}{(2\pi)^2}\, e^{-i\boldsymbol{\Delta}_\perp \cdot \boldsymbol{b}_\perp}\, \frac{P^-}{P^+}\left[-(\sigma_z)_{\lambda'\lambda} G^Z_A(\boldsymbol{\Delta}^2_\perp) + \frac{(\boldsymbol{\Delta}_\perp \cdot \boldsymbol{\sigma}_\perp)_{\lambda'\lambda}}{2M} G^Z_T(\boldsymbol{\Delta}^2_\perp)\right], \\
\boldsymbol{J}^\perp_{5,\text{LF}}(\boldsymbol{b}_\perp; P^+) &= \int \frac{\mathrm{d}^2\boldsymbol{\Delta}_\perp}{(2\pi)^2}\, e^{-i\boldsymbol{\Delta}_\perp \cdot \boldsymbol{b}_\perp}\, \frac{M}{P^+}\Bigg\{ \left[(\boldsymbol{\sigma}_\perp)_{\lambda'\lambda} + \frac{(\boldsymbol{e}_z \times i\boldsymbol{\Delta}_\perp)_\perp}{2M}\delta_{\lambda'\lambda}\right] G^Z_A(\boldsymbol{\Delta}^2_\perp) \\
&\qquad - \frac{\boldsymbol{\Delta}_\perp (\boldsymbol{\Delta}_\perp \cdot \boldsymbol{\sigma}_\perp)_{\lambda'\lambda}}{4M^2} G^Z_P(\boldsymbol{\Delta}^2_\perp)\Bigg\}.
\end{aligned}
$$
(61)

In the case $G^Z_T(\boldsymbol{\Delta}^2_\perp) = 0$, we do explicitly reproduce the LF axial-vector four-current distributions given in Ref. [148]. Again, we confirm that the transverse LF axial-vector current $\boldsymbol{J}^\perp_{5,\text{LF}}$ (61) is independent of the second-class current contribution associated with G^Z_T.

According to Eqs. (61) and (49), one can explicitly show that

$$J_{5,\mathrm{LF}}^{+}(\boldsymbol{b}_{\perp}; P^{+}) = J_{5,\mathrm{EF}}^{0}(\boldsymbol{b}_{\perp}; \infty) = J_{5,\mathrm{EF}}^{z}(\boldsymbol{b}_{\perp}; \infty), \tag{62}$$

where the canonical spin polarizations coincide with the LF helicities in the IMF limit $P_z \to \infty$ (see Sec. VI B). Above result (62) is quite reminiscent of what we have found in the electromagnetic four-current [146] and polarization-magnetization [147] cases. It is therefore clear that for a longitudinally polarized proton, $J_{5,\mathrm{LF}}^{+}(b; P^{+})$ and $2\pi b \cdot J_{5,\mathrm{LF}}^{+}(b; P^{+})$ will be exactly the same as the $P_z = \infty$ case of $J_{5,\mathrm{EF}}^{0}(b; P_z)$ and $2\pi b \cdot J_{5,\mathrm{EF}}^{0}(b; P_z)$ in Fig. 4, respectively. Similarly for a transversely polarized proton, $iJ_{5,\mathrm{LF}}^{+}(b; P^{+})$ and $2\pi b \cdot iJ_{5,\mathrm{LF}}^{+}(b; P^{+})$ will be exactly the same as the $P_z = \infty$ case of $iJ_{5,\mathrm{EF}}^{z}(\boldsymbol{b}_{\perp}; P_z)$ and $2\pi b \cdot iJ_{5,\mathrm{EF}}^{z}(\boldsymbol{b}_{\perp}; P_z)$ in Fig. 5, respectively. In Fig. 9, we illustrate the (scaled) transverse LF axial-vector current distribution $\frac{P^{+}}{M}\boldsymbol{J}_{5,\mathrm{LF}}^{\perp}(\boldsymbol{b}_{\perp}; P^{+})$ in the transverse plane inside a transversely polarized proton, using proton's weak-neutral axial-vector FFs $G_A^Z(Q^2)$ and $G_P^Z(Q^2)$ given in Appendix A. Similarly to Fig. 6, the distribution $\frac{P^{+}}{M}\boldsymbol{J}_{5,\mathrm{LF}}^{\perp}$ in the transverse plane is not mirror symmetric with respect to the x-axis but is still mirror antisymmetric with respect to the y-axis, since $\boldsymbol{J}_{5,\mathrm{LF}}^{\perp}$ also contains monopole, dipole and quadrupole contributions similar as $\boldsymbol{J}_{5,\mathrm{EF}}^{\perp}$.

B. LF amplitudes via proper IMF limit of EF amplitudes

Following Ref. [146], we can explicitly reproduce the LF amplitudes (60) by making use of the EF amplitudes (42) in the *proper* IMF limit (i.e. first keep P^{+} and P^{-} fixed, and then take $P_z \to \infty$ limit). Starting from Eq. (42), we can first construct the following $\mathcal{A}_{\mathrm{EF}}^{+}$ and $\mathcal{A}_{\mathrm{EF}}^{-}$ amplitudes in a generic EF:

$$
\begin{aligned}
\langle p', s'|\hat{j}_5^{+}(0)|p, s\rangle &= \frac{\mathcal{A}_{\mathrm{EF}}^{0} + \mathcal{A}_{\mathrm{EF}}^{z}}{\sqrt{2}} = 2P^{+}\left[(\sigma_z)_{s's}G_A^Z(\boldsymbol{\Delta}_{\perp}^2) + \frac{(\boldsymbol{\sigma}_{\perp}\cdot\boldsymbol{\Delta}_{\perp})_{s's}}{2M}G_T^Z(\boldsymbol{\Delta}_{\perp}^2)\right], \\
\langle p', s'|\hat{j}_5^{+}(0)|p, s\rangle &= \frac{\mathcal{A}_{\mathrm{EF}}^{0} - \mathcal{A}_{\mathrm{EF}}^{z}}{\sqrt{2}} = 2P^{-}\left[-(\sigma_z)_{s's}G_A^Z(\boldsymbol{\Delta}_{\perp}^2) + \frac{(\boldsymbol{\sigma}_{\perp}\cdot\boldsymbol{\Delta}_{\perp})_{s's}}{2M}G_T^Z(\boldsymbol{\Delta}_{\perp}^2)\right],
\end{aligned}
\tag{63}
$$

with $\hat{j}_5^{\pm} \equiv (\hat{j}_5^{0} \pm \hat{j}_5^{z})/\sqrt{2}$. We note that $\langle p', s'|\hat{\boldsymbol{j}}_5^{\perp}(0)|p, s\rangle = \boldsymbol{\mathcal{A}}_{\mathrm{EF}}^{\perp}$ remains the same as in Eq. (42). Above amplitudes $\langle p', s'|\hat{j}_5^{+}(0)|p, s\rangle$ and $\langle p', s'|\hat{j}_5^{+}(0)|p, s\rangle$ clearly are not proper LF amplitudes since they are still defined in terms of the canonical (or instant-form) polarization states $|s\rangle$ rather than the LF helicity states $|\lambda\rangle_{\mathrm{LF}}$ [146].

By keeping P^+ and P^- fixed, we then take the $P_z \to \infty$ limit of $\langle p', s' | \hat{j}_5^+(0) | p, s \rangle$, $\langle p', s' | \hat{j}_5^-(0) | p, s \rangle$ and $\langle p', s' | \hat{\boldsymbol{j}}_5^\perp(0) | p, s \rangle$. It then follows that

$$
\begin{aligned}
\lim_{P_z \to \infty} \langle p', s' | \hat{j}_5^+(0) | p, s \rangle \Big|_{P\pm} &= 2P^+ \left[(\sigma_z)_{s's} G_A^Z(\boldsymbol{\Delta}_\perp^2) + \frac{(\boldsymbol{\sigma}_\perp \cdot \boldsymbol{\Delta}_\perp)_{s's}}{2M} G_T^Z(\boldsymbol{\Delta}_\perp^2) \right], \\
\lim_{P_z \to \infty} \langle p', s' | \hat{j}_5^-(0) | p, s \rangle \Big|_{P\pm} &= P^- \left[-(\sigma_z)_{s's} G_A^Z(\boldsymbol{\Delta}_\perp^2) + \frac{(\boldsymbol{\sigma}_\perp \cdot \boldsymbol{\Delta}_\perp)_{s's}}{2M} G_T^Z(\boldsymbol{\Delta}_\perp^2) \right], \\
\lim_{P_z \to \infty} \langle p', s' | \hat{\boldsymbol{j}}_5^\perp(0) | p, s \rangle \Big|_{P\pm} &= 2M \left[(\boldsymbol{\sigma}_\perp)_{s's} + \frac{(\boldsymbol{e}_z \times i\boldsymbol{\Delta}_\perp)_\perp}{2M} \delta_{s's} \right] G_A^Z(\boldsymbol{\Delta}_\perp^2) \\
&\quad - \frac{\boldsymbol{\Delta}_\perp (\boldsymbol{\Delta}_\perp \cdot \boldsymbol{\sigma}_\perp)_{s's}}{2M} G_P^Z(\boldsymbol{\Delta}_\perp^2),
\end{aligned}
\tag{64}
$$

We note that in the IMF limit (i.e., $P_z \to \infty$), similarly to the electromagnetic case [146], the amplitude $\langle p', s' | \hat{j}_5^+(0) | p, s \rangle$ will be enhanced while the amplitude $\langle p', s' | \hat{j}_5^-(0) | p, s \rangle$ will be suppressed, owing to the associated global factors P^+ and P^-, respectively.

Compared with Eq. (60), we see that above "constructed" EF amplitudes (64) in the proper IMF limit almost coincides with the genuine LF amplitudes (60), except the polarization difference. Recall the fact that canonical polarization states $|s\rangle$ in the $P_z \to \infty$ limit (or equivalently, $M \to 0$ and $Q = |\boldsymbol{\Delta}_\perp| \to 0$ limits) will coincide with the LF helicity states $|\lambda\rangle_{\rm LF}$, namely $\lim_{P_z \to \infty} |s\rangle = |\lambda\rangle_{\rm LF}$ since $\mathcal{M}^{(1/2)}(p) = \mathcal{M}^{\dagger(1/2)}(p') = \mathbb{1}_{2\times 2}$ in the limit $P_z \to \infty$. In other words, we can directly make the following replacements

$$
s \quad \to \quad \lambda, \qquad s' \quad \to \quad \lambda'
\tag{65}
$$

for the "constructed" amplitudes (64) at proper IMF limit. It then follows that

$$
\begin{aligned}
&\lim_{P_z \to \infty} \langle p', s' | \hat{j}_5^+(0) | p, s \rangle \Big|_{P\pm, \, s \to \lambda, \, s' \to \lambda'} \\
&= 2P^+ \left[(\sigma_z)_{\lambda'\lambda} G_A^Z(\boldsymbol{\Delta}_\perp^2) + \frac{(\boldsymbol{\sigma}_\perp \cdot \boldsymbol{\Delta}_\perp)_{\lambda'\lambda}}{2M} G_T^Z(\boldsymbol{\Delta}_\perp^2) \right] = \mathcal{A}_{\rm LF}^+, \\
&\lim_{P_z \to \infty} \langle p', s' | \hat{j}_5^+(0) | p, s \rangle \Big|_{P\pm, \, s \to \lambda, \, s' \to \lambda'} \\
&= 2P^- \left[-(\sigma_z)_{\lambda'\lambda} G_A^Z(\boldsymbol{\Delta}_\perp^2) + \frac{(\boldsymbol{\sigma}_\perp \cdot \boldsymbol{\Delta}_\perp)_{\lambda'\lambda}}{2M} G_T^Z(\boldsymbol{\Delta}_\perp^2) \right] = \mathcal{A}_{\rm LF}^-, \\
&\lim_{P_z \to \infty} \langle p', s' | \hat{\boldsymbol{j}}_5^\perp(0) | p, s \rangle \Big|_{P\pm, \, s \to \lambda, \, s' \to \lambda'} \\
&= 2M \left[(\boldsymbol{\sigma}_\perp)_{\lambda'\lambda} + \frac{(\boldsymbol{e}_z \times i\boldsymbol{\Delta}_\perp)_\perp}{2M} \delta_{\lambda'\lambda} \right] G_A^Z(\boldsymbol{\Delta}_\perp^2) - \frac{\boldsymbol{\Delta}_\perp (\boldsymbol{\Delta}_\perp \cdot \boldsymbol{\sigma}_\perp)_{\lambda'\lambda}}{2M} G_P^Z(\boldsymbol{\Delta}_\perp^2) = \mathcal{A}_{\rm LF}^\perp,
\end{aligned}
\tag{66}
$$

which indeed explicitly coincide with the genuine LF amplitudes (60) as expected [146].

Alternatively, we can also explicitly reproduce the LF amplitudes (60) by using the EF amplitudes in Eqs. (46,48) obtained via the covariant Lorentz transformation (43). Similarly to Eq. (63), we can construct $\langle p', s'|\hat{j}_5^+(0)|p, s\rangle$ and $\langle p', s'|\hat{j}_5^-(0)|p, s\rangle$ from Eq. (46) as follows

$$
\begin{aligned}
\langle p', s'|\hat{j}_5^+(0)|p, s\rangle &= \sqrt{2}(1+\beta)\gamma M\sqrt{1+\tau}\left[\sigma_z G_A^Z(\boldsymbol{\Delta}_\perp^2) + \frac{(\boldsymbol{\sigma}_\perp \cdot \boldsymbol{\Delta}_\perp)}{2M}G_T^Z(\boldsymbol{\Delta}_\perp^2)\right], \\
&= 2P^+\left[\sigma_z G_A^Z(\boldsymbol{\Delta}_\perp^2) + \frac{(\boldsymbol{\sigma}_\perp \cdot \boldsymbol{\Delta}_\perp)}{2M}G_T^Z(\boldsymbol{\Delta}_\perp^2)\right], \\
\langle p', s'|\hat{j}_5^+(0)|p, s\rangle &= \sqrt{2}(1-\beta)\gamma M\sqrt{1+\tau}\left[-\sigma_z G_A^Z(\boldsymbol{\Delta}_\perp^2) + \frac{(\boldsymbol{\sigma}_\perp \cdot \boldsymbol{\Delta}_\perp)}{2M}G_T^Z(\boldsymbol{\Delta}_\perp^2)\right], \\
&= 2P^-\left[-\sigma_z G_A^Z(\boldsymbol{\Delta}_\perp^2) + \frac{(\boldsymbol{\sigma}_\perp \cdot \boldsymbol{\Delta}_\perp)}{2M}G_T^Z(\boldsymbol{\Delta}_\perp^2)\right],
\end{aligned}
\tag{67}
$$

where we have used Eq. (47). Evidently, $\langle p', s'|\hat{\boldsymbol{j}}_5^\perp(0)|p, s\rangle = \boldsymbol{\mathcal{A}}_{\mathrm{EF}}^\perp$ assumes exactly the same expression as in Eq. (48). By taking then the proper IMF limit of $\langle p', s'|\hat{j}_5^+(0)|p, s\rangle$, $\langle p', s'|\hat{j}_5^-(0)|p, s\rangle$ and $\langle p', s'|\hat{\boldsymbol{j}}_5^\perp(0)|p, s\rangle$, we do reproduce Eq. (64) with the help that [146][7]

$$
\lim_{P_z \to \infty} \cos\theta = \frac{1}{\sqrt{1+\tau}}, \qquad \lim_{P_z \to \infty} \sin\theta = -\frac{\sqrt{\tau}}{\sqrt{1+\tau}}.
\tag{68}
$$

Finally, applying the replacements (65) to the "constructed" amplitudes will directly lead to the same LF amplitudes (60). We remind that similar procedure has been used for the cross check of the LF polarization and magnetization amplitudes in Ref. [147].

According to the explicit demonstrations of LF amplitudes via the proper IMF limit of corresponding EF amplitudes in electromagnetic four-current [146], polarization-magnetization tensor [147], and axial-vector four-current (66) cases, we are now confident to propose the following (verified) lemma:

Lemma. *Any light-front (LF) amplitudes for well-defined LF distributions in principle can be explicitly reproduced from the corresponding elastic frame (EF) amplitudes in the proper infinite-momentum frame (IMF) limit (i.e., first keep P^+ and P^- fixed and then take $P_z \to \infty$).*

---

[7] We note that there is a typo in the Eq. (41) of Ref. [146] that "$\lim_{P_z \to \infty} \tan\theta = -1/\sqrt{\tau}$" should be corrected as "$\lim_{P_z \to \infty} \tan\theta = -\sqrt{\tau}$", see Eq. (68).

As a reward, we can classify more easily the origin of distortions appearing in LF distributions in general into three key sources. The first key source of distributions is at amplitude level, originating from complicated Wigner rotations and the mixing of temporal and longitudinal components under longitudinal Lorentz boosts according to the covariant Lorentz transformation (43) for amplitudes from BF to another Lorentz frame (e.g., a generic EF). This is the only source of physical distortions for EF distributions.

The second source of distortions in LF distributions is also at amplitude level, originating from relativistic artefacts caused by Melosh rotations (i.e. the change of Dirac spinors from canonical spin basis to LF helicity basis), see Eq. (55). The change of polarization basis in general affects also the normalization of the amplitudes, which usually brings the P^+-dependence for the transverse components of LF distributions, see e.g. the transverse LF axial-vector current distribution $\boldsymbol{J}^\perp_{5,\mathrm{LF}}(\boldsymbol{b}_\perp; P^+)$ in Eq. (61) and Fig. 9.

The third source of distortions in LF distributions is due to the peculiar LF perspective for defining the LF $\hat{O}^+$ and $\hat{O}^-$ components [146, 147]. The $\hat{O}^+$ component is usually regarded as the "good" component, allowing physically clear probabilistic interpretation [118, 125, 182]. The $\hat{O}^-$ component, however, is usually regarded as the "bad" component, and it is also considered as a complicated object without clear physical interpretation [146] and is therefore often just ignored in the literature.

C.   LF mean-square transverse radii

Similarly to Eq. (51), we can also apply the general definition (50) to the 2D LF axial charge (or helicity) $J^+_{5,\mathrm{LF}}(\boldsymbol{b}_\perp; P^+)$ and longitudinal spin $S_{L,\mathrm{LF}}(\boldsymbol{b}_\perp; P^+) \equiv \frac{1}{4}\mathrm{Tr}\left[\sigma_z J^+_{5,\mathrm{LF}}(\boldsymbol{b}_\perp; P^+)\right]$ distributions (61). It then follows that [181]

$$\langle b^2_A \rangle_{\mathrm{LF}}(P^+) = \langle b^2_{\mathrm{spin},L} \rangle_{\mathrm{LF}}(P^+) = \frac{2}{3}R^2_A, \tag{69}$$

which indeed coincides with Ref. [148]. Besides, since $\boldsymbol{J}^\perp_{5,\mathrm{LF}}$ in Eq. (61) assumes exactly the same expression as in Ref. [148], we then naturally arrive at the same mean-square transverse LF spin radius [148]

$$\langle b^2_{\mathrm{spin},T} \rangle_{\mathrm{LF}}(P^+) = \frac{2}{3}R^2_A + \frac{1}{2M^2}\frac{G^Z_P(0)}{G^Z_A(0)} \tag{70}$$

for the transverse spin distribution $S_{T,\mathrm{LF}}(\boldsymbol{b}_\perp; P^+) \equiv \frac{1}{4}\mathrm{Tr}\left[\boldsymbol{\sigma}_\perp \cdot \boldsymbol{J}_{5,\mathrm{LF}}^\perp(\boldsymbol{b}_\perp; P^+)\right]$. Similarly to what we found in Eqs. (51,52) in the 2D EF case, these LF results (69, 70) again reconfirm that the second-class current contribution associated with the induced (pseudo-)tensor FF $G_T^Z(Q^2)$, although explicitly included in the full matrix elements (59) and $G_T^Z(Q^2)$ indeed enters $J_{5,\mathrm{LF}}^+$, does not contribute in fact to the mean-square transverse axial and spin radii on the LF.

VII. SUMMARY

In this paper, we extended our recent study [148] of the relativistic weak-neutral axial-vector four-current distributions inside a general spin-$\frac{1}{2}$ composite system, where the second-class current contribution associated with the weak-neutral induced (pseudo-)tensor form factor is newly but automatically taken into account in terms of the full matrix elements. To the best of our knowledge, this is the first time that the full weak-neutral axial-vector four-current distributions inside a general spin-$\frac{1}{2}$ system are systematically studied in terms of relativistic Breit frame, elastic frame and light-front distributions.

We explicitly derived the first exact full tree-level unpolarized differential cross sections of both (anti)neutrino-nucleon (15) and (anti)neutrino-antinucleon (21) elastic scatterings in the lab frame using the full vertex functions including 6 weak-neutral form factors, individually. Relative to previous studies, our formulas of the full tree-level unpolarized differential cross sections are more general and complete, and should be more useful for ongoing and future (anti)neutrino-(anti)nucleon elastic scattering experiments.

In particular, we explicitly demonstrated that the relativistic weak-neutral 3D axial charge distribution $J_{5,B}^0$ in the Breit frame is in fact related to the induced (pseudo-)tensor form factor $G_T^Z(Q^2)$ rather than the axial form factor $G_A^Z(Q^2)$. Besides, we newly found that $J_{5,B}^0$ is purely imaginary and parity-odd (33). This can be understood by the fact that $J_{5,B}^0$ is entirely contributed by the second-class current associated with $G_T^Z(Q^2)$ whose existence signs explicitly the G-parity violation, rather by the ordinary first-class current. Owing to the parity-odd nature of $J_{5,B}^0$, the definition of standard mean-square axial (charge) radius (37) is in fact not well-defined. We also tested for the first time the Abel transformation of axial charge distributions in the spin-$\frac{1}{2}$ case, through which we explicitly revealed the breakdown of Abel transformation for the connection in physics between 2D light-front and 3D Breit

frame axial charge distributions, see Appendix B. On the other hand, the 3D axial-vector current distribution $\boldsymbol{J}_{5,B}$ is totally free from the second-class current contribution, and is closely related to the physically meaningful 3D spin distribution (34), from which one can unambiguously define the physically meaningful 3D mean-square spin radius $\langle r_{\text{spin}}^2 \rangle$ which better characterizes the spatial extension of the weak-neutral content of the system [148].

When the system is boosted, the situation gets more complicated since both the Wigner rotation and the mixing of different components under the Lorentz boost will play the roles. We did observe clear frame-dependence of the axial charge distribution $J_{5,\text{EF}}^0$ (longitudinal axial-vector current distribution $J_{5,\text{EF}}^z$) in the generic EF for a longitudinally (transversely) polarized proton. The frame-dependence of $J_{5,\text{EF}}^0$ and $J_{5,\text{EF}}^z$ is solely due to the mixing of temporal and longitudinal components of the axial-vector four-current amplitudes under longitudinal Lorentz boosts (43), since they are both free from the Wigner rotation. On the contrary, the transverse axial-vector current distribution $\boldsymbol{J}_{5,\text{EF}}^\perp$ (49) does not get mixed under longitudinal Lorentz boosts, but it suffers from Wigner rotations (46).

We also studied light-front distributions of full weak-neutral axial-vector four-current. We clarified the role played by Melosh rotations, and further proposed and verified the lemma that *any light-front amplitudes for well-defined light-front distributions in principle can be explicitly reproduced from the corresponding elastic-frame amplitudes in the proper infinite-momentum-frame limit.* As a reward, we can classify more clearly the distortions appearing in light-front distributions into three key sources. For completeness, we rederived both 3D and 2D transverse mean-square axial and spin radii in different frames. We showed in particular that the second-class current contribution, although explicitly included in our calculations, does not contribution in fact to the mean-square axial and spin radii.

To get a more intuitive view of the weak-neutral axial-vector structure of a spin-$\frac{1}{2}$ hadron, we also numerically illustrated our results of the full weak-neutral axial-vector four-current distributions in different frames in the case of a proton, using proton's weak-neutral axial-vector form factors extracted from experimental data, see Appendix A. It should be emphasize that our analytic formulas apply to any spin-$\frac{1}{2}$ hadrons (e.g. Λ^0, Σ^0, Ξ^0, etc.) and can be easily generalized to higher spin systems, as long as the corresponding weak-neutral axial-vector form factors are available.

Appendix A: Parametrization of nucleon weak-neutral axial-vector FFs

In the literature [9, 10, 15, 18, 94], the nucleon weak-neutral $G_A^Z(Q^2)$ and weak-charged $G_A^W(Q^2)$ axial FFs are usually parametrized in terms of a standard dipole model *ansätz*:

$$G_A^L(Q^2) = \frac{G_A^L(0)}{\left(1 + \frac{Q^2}{(M_A^L)^2}\right)^2},\tag{A1}$$

where $L = Z, W$ and M_A^L is the corresponding (axial) dipole mass. We note that the weak-charged nucleon axial FF $G_A^W(Q^2)$ has been extracted from quasielastic (anti)neutrino-nucleon and (anti)neutrino-nuclei scattering data with $M_A^W \approx (1.026 \pm 0.021)\,\mathrm{GeV}$ [94]. The weak-charged axial charge (or coupling constant) $G_A^W(0) = (1.2754 \pm 0.0013)$ [161] is very precisely determined in neutron beta decay reaction $n \to p e^- \bar{\nu}_e$.

According to Refs. [9, 10, 157–160, 183], the weak-neutral axial-vector FFs $G_X^Z(Q^2)$ for $X = A, P, T$ can be related to the corresponding weak-charged ones $G_X^W(Q^2)$ via

$$\begin{aligned}
G_X^Z(Q^2) &= \sum_f g_A^f\, G_X^f(Q^2) \\
&\simeq \frac{1}{2}\left[G_X^W(Q^2) - G_X^s(Q^2) + G_X^c(Q^2) - G_X^b(Q^2) + G_X^t(Q^2)\right],
\end{aligned}\tag{A2}$$

where $G_X^W \simeq G_X^u - G_X^d \equiv G_X^{(u-d)}$, and G_X^f denotes the FF contribution from the f-flavor quark with $f = u, d, s, c, b, t$. We note that the axial-vector couplings of quarks to the Z^0 boson in the Standard Model are given by $g_A^{u,c,t} = \frac{1}{2}$ and $g_A^{d,s,b} = -\frac{1}{2}$, which explains the
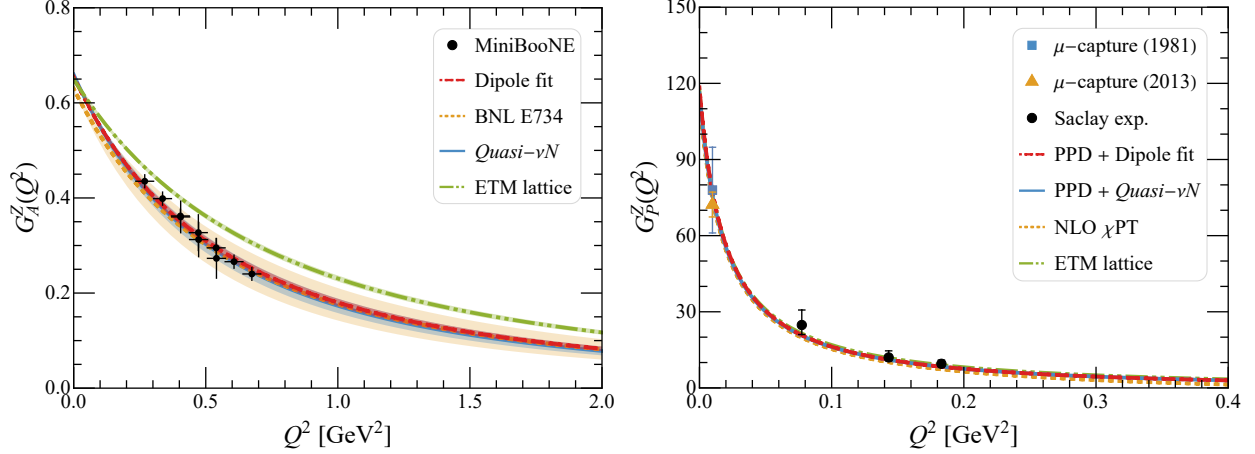
FIG. 10. Comparison of the nucleon weak-neutral axial $G_A^Z(Q^2)$ (left panel) and induced pseudoscalar $G_P^Z(Q^2)$ (right panel) FFs as a function of Q^2 using different methods, where confidence bands of $G_A^Z(Q^2)$ at 95% confidence level are also shown. See texts for more details.

overall factor $\frac{1}{2}$ in Eq. (A2). It should be noted that $G_A^Z(t = -Q^2)$ and $G_P^Z(t = -Q^2)$ can also be accessed via measurements of generalized parton distributions (GPDs) $\tilde{H}_f(x, \xi, t)$ and $\tilde{E}_f(x, \xi, t)$ using facilities at JLab, DESY, CERN, BNL, etc. through the first-moment sum rules [184–186]

$$\begin{bmatrix} G_A^Z(t) \\ G_P^Z(t) \end{bmatrix} = \sum_f g_A^f \int_{-1}^{1} dx \begin{bmatrix} \tilde{H}_f(x, \xi, t) \\ \tilde{E}_f(x, \xi, t) \end{bmatrix}. \tag{A3}$$

In general, the contributions from the heavy-flavor quarks (i.e. c, b, t) are very small for the nucleon and are therefore usually neglected in practical calculations. In this analysis, we also neglect the contributions from heavy-flavor quarks for the nucleon.

Using directly the extracted experimental data of the nucleon weak-neutral axial FF $G_A^Z(Q^2)$ from Ref. [160] based on recent MiniBooNE measurements [15, 18], and performing the standard dipole model (A1) fit to the data (denoted as "Dipole fit"), we find

$$M_A^Z \approx (1.0500 \pm 0.0107) \text{ GeV}, \tag{A4}$$

where $G_A^Z(0) = (0.65520 \pm 0.00465)$ is fixed using both world average experimental data of $G_A^W(0) = (1.2754 \pm 0.0013)$ from Particle Data Table [161] and the strange quark contribution to the nucleon spin $\Delta s \equiv G_A^s(0) \approx (-0.0350 \pm 0.0092)$ in the continuum limit and physical pion point from lattice QCD [187]; see also Refs. [21, 22, 183] for recent analyses of $G_A^s(0)$.

Alternative to Eq. (A1) with M_A^Z given in Eq. (A4), we can also obtain $G_A^Z(Q^2)$ in terms

of $G_A^W(Q^2)$ and $G_A^s(Q^2)$ via Eq. (A2)[8]. For the strange quark contributions $G_A^s(Q^2)$ and $G_P^s(Q^2)$, $G_X^s(Q^2)$ for $X = A, P$ are also parametrized usually in the literature in terms of the standard dipole model [46]

$$G_X^s(Q^2) = \frac{G_X^s(0)}{\left(1 + \frac{Q^2}{(M_X^s)^2}\right)^2}, \tag{A5}$$

where the corresponding dipole parameters $G_A^s(0) = -0.044(8)$, $M_A^s = 0.992(164)$ GeV, $G_P^s(0) = -1.325(406)$ and $M_P^s = 0.609(89)$ GeV taken from Ref. [46].

In the left panel of Fig. 10, we show the direct "Dipole fit" (red dot-dashed curve) result of $G_A^Z(Q^2)$ using the extracted MiniBooNE data [15, 18, 160] (circle markers) via Eq. (A1) and the reconstructed $G_A^Z(Q^2) = [G_A^W(Q^2) - G_A^s(Q^2)]/2$ labeled by "Quasi-νN" (blue solid curve) using Eq. (A2) in terms of G_A^W (A1) extracted from quasi-elastic (anti)neutrino scattering data and G_A^s (A5), in comparison with $G_A^Z(Q^2)$ from the BNL E734 measurements [9, 10] (orange dotted curve) and the recent ETM lattice QCD calculations [44, 46] (green dot-dot-dashed curve), where confidence bands at 95% confidence level are also shown. Within error bands, all these experimental-data-based results (MiniBooNE, Dipole fit, BNL E734, and Quasi-νN) are well consistent with each other, which in turn validates the correctness of Eq. (A2). In contrast, the ETM lattice result of $G_A^Z(Q^2)$ [44, 46] shows sizeable deviation from the MiniBooNE, Dipole fit, BNL E734, and Quasi-νN results.

To the best of our knowledge, there is currently no direct experimental data of the nucleon weak-neutral induced pseudoscalar FF $G_P^Z(Q^2)$ in the literature. To obtain $G_P^Z(Q^2)$, we need the knowledge of $G_P^W(Q^2)$ and $G_P^s(Q^2)$ according to Eq. (A2). The result of $G_P^s(Q^2)$ is given in Eq. (A5) where the dipole parameters can be found in Ref. [46]. The remaining task is to obtain $G_P^W(Q^2)$. In chiral perturbation theory (χPT), the nucleon weak-charged induced pseudoscalar FF $G_P^W(Q^2)$ from full chiral structure up to next-to-leading-order (NLO) is given by [60, 94]

$$G_P^W(Q^2) = g_{\pi^\pm pn} \frac{2(M_p + M_n)F_\pi}{Q^2 + M_\pi^2} - 2G_A^W(0)\frac{(M_p + M_n)^2}{(M_A^W)^2} + \mathcal{O}(Q^2; M_\pi^2), \tag{A6}$$

where $g_{\pi^\pm pn}$ is the pseudoscalar pion-nucleon coupling constant, M_p (M_n) is the proton

---

[8] We note that the direct (anti)neutrino-nucleon elastic scattering data [15, 18, 160] of $G_A^Z(Q^2)$ in turn can help us to test whether the relation (A2) between $G_A^Z(Q^2)$ and $G_A^W(Q^2)$ is valid or not.

(neutron) mass, M_π is the charged pion mass, $F_\pi = f_\pi/\sqrt{2} \approx (92.0653 \pm 0.8485)$ MeV [161] is the pion decay constant for the $\pi^+ \to \mu^+ \nu_\mu$ reaction, and $M_A^W \approx (1.026 \pm 0.021)$ GeV [94]. Based on the recent combined analysis of experimental data using chiral effective field theory for $f_{\pi^\pm pn}^2 = 0.0769(5)^a(0.9)^b$ [188], we find [161]

$$g_{\pi^\pm pn} = \frac{\sqrt{4\pi}(M_p + M_n)}{M_\pi} f_{\pi^\pm pn} \approx (13.22613 \pm 0.04369), \tag{A7}$$

where uncertainties of $f_{\pi^\pm pn}^2$ from the first (a) and second (b) errors are added in quadrature.

Alternatively, we can also obtain $G_P^W(Q^2)$ by assuming the pion-pole dominance (PPD) hypothesis [41, 83], which is based on the low-energy QCD relations—the partially conserved axial-vector current (PCAC) relation and the Goldberger-Treiman relation [189], namely

$$G_P^W(Q^2) = \frac{(M_p + M_n)^2}{M_\pi^2 + Q^2} G_A^W(Q^2), \tag{A8}$$

where $G_A^W(Q^2)$ is extracted from quasielastic (anti)neutrino scattering data [94] via Eq. (A1). We can thus construct $G_P^Z(Q^2) = [G_P^W(Q^2) - G_P^s(Q^2)]/2$ with known $G_P^s(Q^2)$ (A5) by using $G_P^W(Q^2)$ either from Eq. (A6) which is labeled by "NLO χPT", or from Eq. (A8) which is labeled by "PPD + $Quasi$-νN". The PPD hypothesis also inspires us to reconstruct $G_P^Z(Q^2)$ by using directly the "Dipole fit" $G_A^Z(Q^2)$ from Eqs. (A1) and (A4), namely

$$G_P^Z(Q^2) = \frac{4M^2}{M_\pi^2 + Q^2} G_A^Z(Q^2), \tag{A9}$$

which is labeled by "PPD + Dipole fit".

In the right panel of Fig. 10, we present our results of $G_P^Z(Q^2)$ by using different methods: "PPD + Dipole fit" (red dot-dashed curve), "PPD + $Quasi$-νN" (blue solid curve), and "NLO χPT", in comparison with the reconstructed $G_P^Z(Q^2) = [G_P^W(Q^2) - G_P^s(Q^2)]/2$ with $G_P^s(Q^2)$ (A5) by using experimental data of $G_P^W(Q^2)$ from the ordinary μ-capture measurements [190, 191] at[9] $Q^2 \approx 0.88\, M_\mu^2$ in the $\mu^- + p \to n + \nu_\mu$ reaction labeled by "μ-capture (1981)" [190] (square marker) and "μ-capture (2013)" [191] (triangle marker), and from the low-energy charged pion electroproduction measurements [192] labeled by "Saclay exp." (circle markers). Besides, we also show the results of $G_P^Z(Q^2) = [G_P^{(u-d)} - G_P^s]/2$ from the re-

---

[9] More rigorously, $Q^2 = \left[\frac{(M_\mu + M_p)^2 - M_n^2}{M_\mu(M_\mu + M_p)} - 1\right] M_\mu^2 = \left[\frac{M_p(M_\mu + M_p) - M_n^2}{M_\mu(M_\mu + M_p)}\right] M_\mu^2 \approx 0.88\, M_\mu^2$, where M_μ is the muon mass.

cent ETM lattice QCD calculations [44, 46] labeled by "ETM lattice" (green dot-dot-dashed curve). We find that all these results of G_P^Z are well consistent with each other, which also indicates the validity of Eq. (A2). Owing to the intensive overlaps of these results, the confidence bands for $G_P^Z(Q^2)$ at 95% confidence level are not shown.

For the nucleon weak-neutral induced (pseudo-)tensor FF G_T^Z, there is currently no direct experimental data at all. To some extent, this is also the reason why the second-class current contribution of the nucleon associated with the induced (pseudo-)tensor FF $G_T^Z(Q^2)$ are scarcely discussed and calculated in the literature [58–60, 63–85, 87]. According to the Fig. 7 of Ref. [172], one can assume that $G_T^W(Q^2)$ can by roughly approximated by $G_T^W(Q^2) \equiv \kappa_T G_A^W(Q^2)$, where the factor $\kappa_T \approx 0.1$ is roughly the mean value of the ratio $G_T^W(0)/G_A^W(0)$ in the Fig. 7 of Ref. [172] with $G_A^W = F_A$ and $G_T^W = 2F_A^3$, and $G_A^W(Q^2)$ is given in Eq. (A1) with $M_A^W \approx (1.026 \pm 0.021) \, \text{GeV}$ [94].

As a reward, Ref. [172] thus inspires us to propose the following *ansätz* for the nucleon weak-neutral induced (pseudo-)tensor FF $G_T^Z(Q^2)$:

$$G_T^W(Q^2) = \kappa_T G_A^Z(Q^2), \tag{A10}$$

where $G_A^Z(Q^2)$ is the direct dipole model (A1) fit to the elastic (anti)neutrino-nucleon scattering data [15, 18, 160]. We should emphasize that the reason why we relate $G_T^Z(Q^2)$ with $G_A^Z(Q^2)$ via the *ansätz* (A10) is simply because the assumption proposed in Ref. [172], which is the *only* reference that we have ever found with experimentally reasonable and useful relation for $G_T^W(Q^2)$ [and thus for $G_T^Z(Q^2)$]. In the real word, $G_T^Z(Q^2)$ is most probably to be quite different from $G_A^Z(Q^2)$ instead of the simple but naive scaling *ansätz* (A10), since $G_T^Z(Q^2)$ is strongly constrained by many symmetries and conservation laws while $G_A^Z(Q^2)$ is not. This provides also a key motivation for future experimental measurements of $G_T^Z(Q^2)$ and $G_T^W(Q^2)$ for the nucleon in (anti)neutrino-nucleon elastic and quasielastic scatterings, respectively, e.g. using the full tree-level unpolarized differential cross sections (15).

For numerical calculations and illustrations of the nucleon weak-neutral axial-vector four-current distributions in Sec. IV to Sec. VI, we declare that we employ only nucleon weak-neutral axial-vector FFs $G_A^Z(Q^2)$ from Eq. (A1) via the "Dipole fit", $G_P^Z(Q^2)$ from Eq. (A9) using the "Dipole fit" $G_A^Z(Q^2)$ and the PPD hypothesis (A9), and $G_T^Z(Q^2)$ from Eq. (A10) using the "Dipole fit" $G_A^Z(Q^2)$ and $\kappa_T \approx 0.1$.

Appendix B: Breakdown of Abel transformation for axial charge distributions

The Abel and its inverse transforms, named after Niels H. Abel for integral transforms in mathematics, have been visited recently in several works [177, 178, 193–197] in the case of charge and energy-momentum tensor spatial distributions with the goal of connecting 2D LF spatial distributions with the corresponding 3D ones, where 2D LF spatial distributions are regarded as the 2D Abel images of the corresponds 3D spatial distributions. We notice that some discussions and debates have already been triggered in Refs. [194, 198]. In this appendix, we will explicitly show the breakdown of Abel and its inverse transforms for the connection between 2D LF and 3D BF axial charge distributions in the spin-$\frac{1}{2}$ case.

According to textbooks, the standard definitions of the Abel and its inverse transforms are given by [199]

$$
\mathscr{A}[g](b) \equiv \mathcal{G}(b) = 2 \int_b^\infty \mathrm{d}r \frac{r}{\sqrt{r^2 - b^2}} g(r),
$$
$$
g(r) = -\frac{1}{\pi} \int_r^\infty \mathrm{d}b \frac{1}{\sqrt{b^2 - r^2}} \frac{\mathrm{d}\mathcal{G}(b)}{\mathrm{d}b},
\tag{B1}
$$

where $\mathscr{A}[g](b) \equiv \mathcal{G}(b)$ is called the 2D Abel image of the 3D spatial function $g(r)$ [198]. It is thus not difficult to obtain the following generic relation for the nth order Mellin moment of the Abel image $\mathcal{G}(b)$ in connecting with the corresponding 3D spatial function $g(r)$:

$$
\int_0^\infty \mathrm{d}b\, b^{n-1} \mathcal{G}(b) = \frac{\sqrt{\pi}\, \Gamma\left(\frac{n}{2}\right)}{\Gamma\left(\frac{n+1}{2}\right)} \int_0^\infty \mathrm{d}r\, r^n g(r), \qquad n \in \mathbb{N}^+ = \{1, 2, 3, \cdots\}, \tag{B2}
$$

which is believed to be valid as long as $g(r)$ decreases faster than any order of r^n [177].

Using the dipole model *ansätz* (A1) for the axial FF $G_A^Z(Q^2)$, one can easily obtain the following analytic expression of the LF axial charge distribution from Eq. (61) for a longitudinally polarized spin-$\frac{1}{2}$ target (with $b = |\boldsymbol{b}_\perp|$):

$$
J_{5,\mathrm{LF}}^+(\boldsymbol{b}_\perp; P^+) = (\sigma_z)_{\lambda'\lambda} G_A^Z(0) \frac{b(M_A^Z)^3}{4\pi} K_1(bM_A^Z) \equiv J_{5,\mathrm{LF}}^+(b), \tag{B3}
$$

which is axially symmetric and can be regarded as the 2D Abel image of a 3D spatial distribution $J_{5,\mathrm{naive}}^0(r)$. Applying the inverse Abel transform (B1) to $J_{5,\mathrm{LF}}^+(b)$, we find

$$
J_{5,\mathrm{naive}}^0(r) = (\sigma_z)_{\lambda'\lambda} G_A^Z(0) \frac{(M_A^Z)^3}{8\pi} e^{-rM_A^Z}. \tag{B4}
$$

One can first check that the axial charge normalization condition

$$(\sigma_z)_{\lambda'\lambda} G_A^Z(0) = \int \mathrm{d}^3 r \, J_{5,\text{naive}}^0(r) = \int \mathrm{d}^2 b_\perp \, J_{5,\text{LF}}^+(b) \tag{B5}$$

seems to be automatically guaranteed. Besides, one can also check that $J_{5,\text{LF}}^+(b)$ and $J_{5,\text{naive}}^0(r)$ indeed satisfy the generic relation (B2) for the corresponding Mellin moment at any order. In particular, we find that the mean-square axial (charge) radius of $J_{5,\text{naive}}^0(r)$ is given by

$$\langle r_A^2 \rangle_{\text{naive}}^{\text{Abel}} = \frac{\int \mathrm{d}^3 r \, r^2 J_{5,\text{naive}}^0(r)}{\int \mathrm{d}^3 r \, J_{5,\text{naive}}^0(r)} = \frac{12}{(M_A^Z)^2} \approx (0.6510 \text{ fm})^2$$
$$= -\frac{6}{G_A^Z(0)} \frac{\mathrm{d} G_A^Z(Q^2)}{\mathrm{d} Q^2}\bigg|_{Q^2=0} = R_A^2, \tag{B6}$$

which exactly coincides with the identification of R_A^2 via Eq. (38) widely employed in the literature [19, 20, 58, 59, 104, 173–176]. In contrast to $J_{5,\text{naive}}^0$ (B4), the *genuine* 3D axial charge distribution (33) for a longitudinally polarized target is in fact given by

$$J_{5,B}^0(\boldsymbol{r}) = (\sigma_z)_{s's} \int \frac{\mathrm{d}^3 \Delta}{(2\pi)^3} \, e^{-i\boldsymbol{\Delta}\cdot\boldsymbol{r}} \frac{\Delta_z}{2M} G_T^Z(\boldsymbol{\Delta}^2), \tag{B7}$$

which is actually related to the induced (pseudo-)tensor FF $G_T^Z(Q^2)$ rather than the axial FF $G_A^Z(Q^2)$. This explicitly demonstrates that even though we neglect the polarization difference, the naive 3D distribution $J_{5,\text{naive}}^0(r)$ does not assume clear physical meaning for quantifying the genuine 3D spatial distribution of weak-neutral axial charges in the BF for a longitudinally polarized spin-$\frac{1}{2}$ target. This explicitly reveals for the first time the breakdown of Abel and its inverse transforms for the connection in physics between 2D LF and 3D BF axial charge distributions in the spin-$\frac{1}{2}$ case. It should be noted that some discussions on the breakdown of Abel transformations for targets with spin $j \geq 1$ have recently been presented in Ref. [198].

[1] H. Gao and M. Vanderhaeghen, Rev. Mod. Phys. **94**, 015002 (2022).

[2] R. Li *et al.*, Nature (2022), 10.1038/s41586-022-05248-1, arXiv:2210.11461 [nucl-ex].

[3] S. K. Singh, Nucl. Phys. B **36**, 419 (1972).

[4] W. A. Mann *et al.*, Phys. Rev. Lett. **31**, 844 (1973).

[5] S. J. Barish *et al.*, Phys. Rev. D **16**, 3103 (1977).

[6] N. J. Baker, A. M. Cnops, P. L. Connolly, S. A. Kahn, H. G. Kirk, M. J. Murtagh, R. B. Palmer, N. P. Samios, and M. Tanaka, Phys. Rev. D **23**, 2499 (1981).

[7] K. L. Miller *et al.*, Phys. Rev. D **26**, 537 (1982).

[8] T. Kitagaki *et al.*, Phys. Rev. D **28**, 436 (1983).

[9] J. Horstkotte, A. Entenberg, R. S. Galik, A. K. Mann, H. H. Williams, W. Kozanecki, C. Rubbia, J. Strait, L. Sulak, and P. J. Wanderer, Phys. Rev. D **25**, 2743 (1982).

[10] L. A. Ahrens *et al.*, Phys. Rev. D **35**, 785 (1987).

[11] D. Allasia *et al.*, Nucl. Phys. B **343**, 285 (1990).

[12] T. Kitagaki *et al.*, Phys. Rev. D **42**, 1331 (1990).

[13] R. Gran *et al.* (K2K Collaboration), Phys. Rev. D **74**, 052002 (2006), arXiv:hep-ex/0603034.

[14] A. A. Aguilar-Arevalo *et al.* (MiniBooNE Collaboration), Phys. Rev. D **81**, 092005 (2010), arXiv:1002.2680 [hep-ex].

[15] A. A. Aguilar-Arevalo *et al.* (MiniBooNE Collaboration), Phys. Rev. D **82**, 092005 (2010), arXiv:1007.4730 [hep-ex].

[16] K. Park *et al.* (CLAS Collaboration), Phys. Rev. C **85**, 035208 (2012), arXiv:1201.0903 [nucl-ex].

[17] L. Fields *et al.* (MINERνA Collaboration), Phys. Rev. Lett. **111**, 022501 (2013), arXiv:1305.2234 [hep-ex].

[18] A. A. Aguilar-Arevalo *et al.* (MiniBooNE Collaboration), Phys. Rev. D **91**, 012004 (2015), arXiv:1309.7257 [hep-ex].

[19] A. S. Meyer, M. Betancourt, R. Gran, and R. J. Hill, Phys. Rev. D **93**, 113015 (2016), arXiv:1603.03048 [hep-ph].

[20] T. Cai *et al.* (MINERνA Collaboration), Nature **614**, 48 (2023).

[21] S. F. Pate, D. W. McKee, and V. Papavassiliou, Phys. Rev. C **78**, 015207 (2008), arXiv:0805.2889 [hep-ex].

[22] S. F. Pate, V. Papavassiliou, J. P. Schaub, D. P. Trujillo, M. V. Ivanov, M. B. Barbaro, and C. Giusti, Phys. Rev. D **109**, 093001 (2024), arXiv:2402.10854 [hep-ph].

[23] N. Agafonova *et al.* (OPERA Collaboration), Phys. Rev. D **100**, 051301 (2019).

[24] H. de Kerret *et al.* (Double Chooz Collaboration), Nature Phys. **16**, 558 (2020), arXiv:1901.09445 [hep-ex].

[25] K. Abe *et al.* (T2K, Super-Kamiokande Collaboration), (2024), arXiv:2405.12488 [hep-ex].

[26] A. Abed Abud *et al.* (DUNE Collaboration), (2024), arXiv:2408.12725 [physics.ins-det].

[27] S. Abe *et al.* (KamLAND Collaboration), Phys. Rev. D **107**, 072006 (2023).

[28] F. P. An *et al.* (Daya Bay Collaboration), Phys. Rev. Lett. **133**, 051801 (2024).

[29] R. Abbasi *et al.* (IceCube Collaboration), (2024), arXiv:2405.02163 [hep-ex].

[30] A. Abusleme *et al.* (JUNO Collaboration), (2024), arXiv:2405.18008 [hep-ex].

[31] M. A. Acero *et al.* (NOvA Collaboration), (2024), arXiv:2409.04553 [hep-ex].

[32] T. Bhattacharya, V. Cirigliano, S. Cohen, R. Gupta, H.-W. Lin, and B. Yoon, Phys. Rev. D **94**, 054508 (2016), arXiv:1606.07049 [hep-lat].

[33] J. Liang, Y.-B. Yang, K.-F. Liu, A. Alexandru, T. Draper, and R. S. Sufian, Phys. Rev. D **96**, 034519 (2017), arXiv:1612.04388 [hep-lat].

[34] J. Green, N. Hasan, S. Meinel, M. Engelhardt, S. Krieg, J. Laeuchli, J. Negele, K. Orginos, A. Pochinsky, and S. Syritsyn, Phys. Rev. D **95**, 114502 (2017), arXiv:1703.06703 [hep-lat].

[35] R. Gupta, Y.-C. Jang, H.-W. Lin, B. Yoon, and T. Bhattacharya, Phys. Rev. D **96**, 114503 (2017), arXiv:1705.06834 [hep-lat].

[36] D.-L. Yao, L. Alvarez-Ruso, and M. J. Vicente-Vacas, Phys. Rev. D **96**, 116022 (2017), arXiv:1708.08776 [hep-ph].

[37] N. Hasan, J. Green, S. Meinel, M. Engelhardt, S. Krieg, J. Negele, A. Pochinsky, and S. Syritsyn, Phys. Rev. D **97**, 034504 (2018), arXiv:1711.11385 [hep-lat].

[38] K.-I. Ishikawa, Y. Kuramashi, S. Sasaki, N. Tsukamoto, A. Ukawa, and T. Yamazaki (PACS Collaboration), Phys. Rev. D **98**, 074510 (2018), arXiv:1807.03974 [hep-lat].

[39] E. Shintani, K.-I. Ishikawa, Y. Kuramashi, S. Sasaki, and T. Yamazaki, Phys. Rev. D **99**, 014510 (2019), [Erratum: Phys.Rev.D 102, 019902 (2020)], arXiv:1811.07292 [hep-lat].

[40] N. Hasan, J. Green, S. Meinel, M. Engelhardt, S. Krieg, J. Negele, A. Pochinsky, and S. Syritsyn, Phys. Rev. D **99**, 114505 (2019), arXiv:1903.06487 [hep-lat].

[41] Y.-C. Jang, R. Gupta, B. Yoon, and T. Bhattacharya, Phys. Rev. Lett. **124**, 072002 (2020), arXiv:1905.06470 [hep-lat].

[42] G. S. Bali, L. Barca, S. Collins, M. Gruber, M. Löffler, A. Schäfer, W. Söldner, P. Wein, S. Weishäupl, and T. Wurm (RQCD Collaboration), JHEP **05**, 126 (2020), arXiv:1911.13150 [hep-lat].

[43] H.-W. Lin, Phys. Rev. Lett. **127**, 182001 (2021), arXiv:2008.12474 [hep-ph].

[44] C. Alexandrou *et al.*, Phys. Rev. D **103**, 034509 (2021), arXiv:2011.13342 [hep-lat].

[45] S. Park, R. Gupta, B. Yoon, S. Mondal, T. Bhattacharya, Y.-C. Jang, B. Joó, and F. Winter (NME Collaboration), Phys. Rev. D **105**, 054505 (2022), arXiv:2103.05599 [hep-lat].

[46] C. Alexandrou, S. Bacchio, M. Constantinou, K. Hadjiyiannakou, K. Jansen, and G. Koutsou, Phys. Rev. D **104**, 074503 (2021), arXiv:2106.13468 [hep-lat].

[47] K.-I. Ishikawa, Y. Kuramashi, S. Sasaki, E. Shintani, and T. Yamazaki (PACS Collaboration), Phys. Rev. D **104**, 074514 (2021), arXiv:2107.07085 [hep-lat].

[48] A. S. Meyer *et al.*, PoS **LATTICE2021**, 081 (2022), arXiv:2111.06333 [hep-lat].

[49] T. Schulz, D. Djukanovic, G. von Hippel, J. Koponen, H. B. Meyer, K. Ottnad, and H. Wittig, PoS **LATTICE2021**, 577 (2022), arXiv:2112.00127 [hep-lat].

[50] C. Alexandrou, S. Bacchio, M. Constantinou, J. Finkenrath, K. Hadjiyiannakou, K. Jansen, G. Koutsou, and A. Vaquero, PoS **LATTICE2021**, 250 (2022), arXiv:2112.06750 [hep-lat].

[51] H.-W. Lin, Phys. Lett. B **824**, 136821 (2022), arXiv:2112.07519 [hep-lat].

[52] C. Alexandrou, SciPost Phys. Proc. **6**, 006 (2022).

[53] D. Djukanovic, G. von Hippel, J. Koponen, H. B. Meyer, K. Ottnad, T. Schulz, and H. Wittig, Phys. Rev. D **106**, 074503 (2022), arXiv:2207.03440 [hep-lat].

[54] H.-W. Lin, Few Body Syst. **63**, 65 (2022).

[55] J. Koponen, D. Djukanovic, G. von Hippel, H. B. Meyer, K. Ottnad, T. Schulz, and H. Wittig, PoS **LATTICE2022**, 113 (2023).

[56] Y.-C. Jang, R. Gupta, T. Bhattacharya, B. Yoon, and H.-W. Lin (PNDME Collaboration), Phys. Rev. D **109**, 014503 (2024).

[57] C. Alexandrou, S. Bacchio, M. Constantinou, J. Finkenrath, R. Frezzotti, B. Kostrzewa, G. Koutsou, G. Spanoudes, and C. Urbach (Extended Twisted Mass Collaboration), Phys. Rev. D **109**, 034503 (2024).

[58] U. G. Meissner and N. Kaiser, Phys. Lett. B **180**, 129 (1986).

[59] U. G. Meissner, N. Kaiser, and W. Weise, Nucl. Phys. A **466**, 685 (1987).

[60] V. Bernard, N. Kaiser, and U. G. Meissner, Phys. Rev. D **50**, 6899 (1994), arXiv:hep-ph/9403351.

[61] T. Ohlsson and H. Snellman, Eur. Phys. J. C **6**, 285 (1999), arXiv:hep-ph/9803490.

[62] D. Barquilla-Cano, A. J. Buchmann, and E. Hernandez, Nucl. Phys. A **714**, 611 (2003), arXiv:nucl-th/0204067.

[63] A. Silva, H.-C. Kim, D. Urbano, and K. Goeke, Phys. Rev. D **72**, 094011 (2005).

[64] M. R. Schindler and S. Scherer, Eur. Phys. J. A **32**, 429 (2007), arXiv:hep-ph/0608325.

[65] T. M. Aliev and M. Savci, Phys. Lett. B **656**, 56 (2007), arXiv:0711.1757 [hep-ph].

[66] N. Sharma, H. Dahiya, P. K. Chatley, and M. Gupta, Phys. Rev. D **79**, 077503 (2009), arXiv:0904.2246 [hep-ph].

[67] G. Eichmann and C. S. Fischer, Eur. Phys. J. A **48**, 9 (2012), arXiv:1111.2614 [hep-ph].

[68] X. Y. Liu, K. Khosonthongkee, A. Limphirat, P. Suebka, and Y. Yan, Phys. Rev. D **91**, 034022 (2015), arXiv:1406.7633 [hep-ph].

[69] H. Dahiya and M. Randhawa, Phys. Rev. D **90**, 074001 (2014), arXiv:1409.4943 [hep-ph].

[70] G. Ramalho and K. Tsushima, Phys. Rev. D **94**, 014001 (2016), arXiv:1512.01167 [hep-ph].

[71] I. V. Anikin, V. M. Braun, and N. Offen, Phys. Rev. D **94**, 034011 (2016).

[72] S. Mamedov, B. B. Sirvanli, I. Atayev, and N. Huseynova, Int. J. Theor. Phys. **56**, 1861 (2017), arXiv:1609.00167 [hep-th].

[73] H. Hashamipour, M. Goharipour, and S. S. Gousheh, Phys. Rev. D **100**, 016001 (2019), arXiv:1903.05542 [hep-ph].

[74] C. Mondal, S. Xu, J. Lan, X. Zhao, Y. Li, D. Chakrabarti, and J. P. Vary, Phys. Rev. D **102**, 016008 (2020), arXiv:1911.10913 [hep-ph].

[75] X. Zhang, T. J. Hobbs, and G. A. Miller, Phys. Rev. D **102**, 074026 (2020).

[76] Y.-S. Jun, J.-M. Suh, and H.-C. Kim, Phys. Rev. D **102**, 054011 (2020).

[77] C. Chen, C. S. Fischer, C. D. Roberts, and J. Segovia, Phys. Lett. B **815**, 136150 (2021), arXiv:2011.14026 [hep-ph].

[78] C. Chen, C. S. Fischer, C. D. Roberts, and J. Segovia, Phys. Rev. D **105**, 094022 (2022), arXiv:2103.02054 [hep-ph].

[79] M. Ahmady, D. Chakrabarti, C. Mondal, and R. Sandapen, Nucl. Phys. A **1016**, 122334 (2021), arXiv:2105.02213 [hep-ph].

[80] U. Sauerwein, M. F. M. Lutz, and R. G. E. Timmermans, Phys. Rev. D **105**, 054005 (2022), arXiv:2105.06755 [hep-ph].

[81] S. Xu, C. Mondal, J. Lan, X. Zhao, Y. Li, and J. P. Vary (BLFQ Collaboration), Phys. Rev. D **104**, 094036 (2021), arXiv:2108.03909 [hep-ph].

[82] I. Atayev and S. Mamedov, Int. J. Theor. Phys. **61**, 250 (2022), arXiv:2205.14958 [hep-ph].

[83] C. Chen and C. D. Roberts, Eur. Phys. J. A **58**, 206 (2022), arXiv:2206.12518 [hep-ph].

[84] P. Cheng, F. E. Serna, Z.-Q. Yao, C. Chen, Z.-F. Cui, and C. D. Roberts, Phys. Rev. D **106**, 054031 (2022), arXiv:2207.13811 [hep-ph].

[85] X. Y. Liu, A. Limphirat, K. Xu, Z. Zhao, K. Khosonthongkee, and Y. Yan, Phys. Rev. D **107**, 074006 (2023), arXiv:2209.00808 [hep-ph].

[86] F. Irani, M. Goharipour, H. Hashamipour, and K. Azizi, Phys. Rev. D **108**, 074018 (2023).

[87] G. Ramalho, K. Tsushima, and M.-K. Cheoun, arXiv:2406.07958 [hep-ph].

[88] O. Tomalak, Q. Chen, R. J. Hill, K. S. McFarland, and C. Wret, Phys. Rev. D **106**, 093006 (2022), arXiv:2204.11379 [hep-ph].

[89] J. E. Sobczyk and J. Nieves, (2024), arXiv:2407.21587 [nucl-th].

[90] M. Sajjad Athar, A. Fatima, S. K. Singh, and F. Zaidi, (2024), arXiv:2409.14732 [hep-ph].

[91] C. H. Llewellyn Smith, Phys. Rept. **3**, 261 (1972).

[92] M. Gourdin, Phys. Rept. **11**, 29 (1974).

[93] V. Bernard, N. Kaiser, and U.-G. Meissner, Int. J. Mod. Phys. E **4**, 193 (1995).

[94] V. Bernard, L. Elouadrhiri, and U.-G. Meissner, J. Phys. G **28**, R1 (2002), arXiv:hep-ph/0107088.

[95] T. Gorringe and H. W. Fearing, Rev. Mod. Phys. **76**, 31 (2004), arXiv:nucl-th/0206039.

[96] E. J. Beise, M. L. Pitt, and D. T. Spayde, Prog. Part. Nucl. Phys. **54**, 289 (2005), arXiv:nucl-ex/0412054.

[97] H. Gallagher, G. Garvey, and G. P. Zeller, Ann. Rev. Nucl. Part. Sci. **61**, 355 (2011).

[98] J. A. Formaggio and G. P. Zeller, Rev. Mod. Phys. **84**, 1307 (2012), arXiv:1305.7513 [hep-ex].

[99] J. G. Morfin, J. Nieves, and J. T. Sobczyk, Adv. High Energy Phys. **2012**, 934597 (2012), arXiv:1209.6586 [hep-ex].

[100] R. Gonzalez-Jimenez, J. A. Caballero, and T. W. Donnelly, Phys. Rept. **524**, 1 (2013), arXiv:1111.6918 [nucl-th].

[101] L. Alvarez-Ruso, Y. Hayato, and J. Nieves, New J. Phys. **16**, 075015 (2014).

[102] U. Mosel, Ann. Rev. Nucl. Part. Sci. **66**, 171 (2016), arXiv:1602.00696 [nucl-th].

[103] L. Alvarez-Ruso *et al.* (NuSTEC Collaboration), Prog. Part. Nucl. Phys. **100**, 1 (2018), arXiv:1706.03621 [hep-ph].

[104] R. J. Hill, P. Kammel, W. J. Marciano, and A. Sirlin, Rept. Prog. Phys. **81**, 096301 (2018), arXiv:1708.08462 [hep-ph].

[105] A. S. Meyer, A. Walker-Loud, and C. Wilkinson, Ann. Rev. Nucl. Part. Sci. **72**, 205 (2022),

arXiv:2201.01839 [hep-lat].

[106] M. Sajjad Athar, A. Fatima, and S. K. Singh, Prog. Part. Nucl. Phys. **129**, 104019 (2023), arXiv:2206.13792 [hep-ph].

[107] F. J. Ernst, R. G. Sachs, and K. C. Wali, Phys. Rev. **119**, 1105 (1960).

[108] R. G. Sachs, Phys. Rev. **126**, 2256 (1962).

[109] D. R. Yennie, M. M. Lévy, and D. G. Ravenhall, Rev. Mod. Phys. **29**, 144 (1957).

[110] G. Breit, in *Proceedings of the XII International Conference on High Energy Physics (ICHEP 1964)* (Atomizdat, Moscow, 1966) pp. 985–987.

[111] J. J. Kelly, Phys. Rev. C **66**, 065203 (2002).

[112] M. Burkardt, Phys. Rev. D **62**, 071503 (2000), [Erratum: Phys.Rev.D 66, 119903 (2002)].

[113] A. V. Belitsky, X.-d. Ji, and F. Yuan, Phys. Rev. D **69**, 074014 (2004).

[114] R. L. Jaffe, Phys. Rev. D **103**, 016017 (2021).

[115] S. J. Brodsky, H.-C. Pauli, and S. S. Pinsky, Phys. Rept. **301**, 299 (1998).

[116] L. Susskind, Phys. Rev. **165**, 1535 (1968).

[117] J. B. Kogut and D. E. Soper, Phys. Rev. D **1**, 2901 (1970).

[118] M. Burkardt, Int. J. Mod. Phys. A **18**, 173 (2003).

[119] G. A. Miller, Phys. Rev. Lett. **99**, 112001 (2007).

[120] C. E. Carlson and M. Vanderhaeghen, Phys. Rev. Lett. **100**, 032004 (2008).

[121] C. Alexandrou, T. Korzec, G. Koutsou, T. Leontiou, C. Lorcé, J. W. Negele, V. Pascalutsa, A. Tsapalis, and M. Vanderhaeghen, Phys. Rev. D **79**, 014507 (2009).

[122] C. Alexandrou, T. Korzec, G. Koutsou, C. Lorcé, J. W. Negele, V. Pascalutsa, A. Tsapalis, and M. Vanderhaeghen, Nucl. Phys. A **825**, 115 (2009).

[123] C. E. Carlson and M. Vanderhaeghen, Eur. Phys. J. A **41**, 1 (2009).

[124] M. Gorchtein, C. Lorcé, B. Pasquini, and M. Vanderhaeghen, Phys. Rev. Lett. **104**, 112001 (2010).

[125] G. A. Miller, Ann. Rev. Nucl. Part. Sci. **60**, 1 (2010).

[126] G. A. Miller, Phys. Rev. C **99**, 035202 (2019).

[127] A. Freese and G. A. Miller, Phys. Rev. D **107**, 074036 (2023), arXiv:2302.09171 [hep-ph].

[128] A. Freese and G. A. Miller, Phys. Rev. D **108**, 094026 (2023), arXiv:2307.11165 [hep-ph].

[129] G. A. Miller and S. J. Brodsky, Phys. Rev. C **102**, 022201 (2020), arXiv:1912.08911 [hep-ph].

[130] M. Jacob and G. C. Wick, Ann. Phys. (N.Y.) **7**, 404 (1959).

[131] L. Durand, P. C. DeCelles, and R. B. Marr, Phys. Rev. **126**, 1882 (1962).

[132] H. J. Melosh, Phys. Rev. D **9**, 1095 (1974).

[133] C. Lorce and B. Pasquini, Phys. Rev. D **84**, 034039 (2011), arXiv:1104.5651 [hep-ph].

[134] W. N. Polyzou, W. Glöckle, and H. Witala, Few Body Syst. **54**, 1667 (2013).

[135] Z. Li, M. An, and C.-R. Ji, Phys. Rev. D **92**, 105014 (2015), arXiv:1509.00431 [hep-th].

[136] E. P. Wigner, Phys. Rev. **40**, 749 (1932).

[137] M. Hillery, R. F. O'Connell, M. O. Scully, and E. P. Wigner, Phys. Rept. **106**, 121 (1984).

[138] I. Bialynicki-Birula, P. Gornicki, and J. Rafelski, Phys. Rev. D **44**, 1825 (1991).

[139] C. Lorcé, L. Mantovani, and B. Pasquini, Phys. Lett. B **776**, 38 (2018).

[140] C. Lorcé, Eur. Phys. J. C **78**, 785 (2018).

[141] C. Lorcé, H. Moutarde, and A. P. Trawiński, Eur. Phys. J. C **79**, 89 (2019).

[142] C. Lorcé, Phys. Rev. Lett. **125**, 232002 (2020), arXiv:2007.05318 [hep-ph].

[143] C. Lorcé, Eur. Phys. J. C **81**, 413 (2021).

[144] C. Lorcé and P. Wang, Phys. Rev. D **105**, 096032 (2022), arXiv:2204.01465 [hep-ph].

[145] C. Lorcé, P. Schweitzer, and K. Tezgin, Phys. Rev. D **106**, 014012 (2022).

[146] Y. Chen and C. Lorcé, Phys. Rev. D **106**, 116024 (2022), arXiv:2210.02908 [hep-ph].

[147] Y. Chen and C. Lorcé, Phys. Rev. D **107**, 096003 (2023), arXiv:2302.04672 [hep-ph].

[148] Y. Chen, Y. Li, C. Lorcé, and Q. Wang, (2024), arXiv:2405.12943 [hep-ph].

[149] K.-H. Hong, J.-Y. Kim, and H.-C. Kim, Phys. Rev. D **107**, 074004 (2023).

[150] S. Weinberg, Phys. Rev. **112**, 1375 (1958).

[151] J. S. Schwinger, Annals Phys. **2**, 407 (1957).

[152] T. D. Lee and C.-N. Yang, Phys. Rev. **108**, 1611 (1957).

[153] R. P. Feynman and M. Gell-Mann, Phys. Rev. **109**, 193 (1958).

[154] S. K. Singh and M. J. Vicente Vacas, Phys. Rev. D **74**, 053009 (2006), arXiv:hep-ph/0606235.

[155] A. Fatima, M. Sajjad Athar, and S. K. Singh, Phys. Rev. D **98**, 033005 (2018), arXiv:1806.08597 [hep-ph].

[156] B. R. Holstein, Phys. Rev. C **29**, 623 (1984).

[157] S. Weinberg, Phys. Rev. D **5**, 1412 (1972).

[158] G. T. Garvey, W. C. Louis, and D. H. White, Phys. Rev. C **48**, 761 (1993).

[159] G. Garvey, E. Kolbe, K. Langanke, and S. Krewald, Phys. Rev. C **48**, 1919 (1993).

[160] R. S. Sufian, K.-F. Liu, and D. G. Richards, JHEP **01**, 136 (2020).

[161] S. Navas *et al.* (Particle Data Group Collaboration), Phys. Rev. D **110**, 030001 (2024).

[162] M. H. L. Pryce, Proc. Roy. Soc. Lond. A **195**, 62 (1948).

[163] T. D. Newton and E. P. Wigner, Rev. Mod. Phys. **21**, 400 (1949).

[164] L. L. Foldy and S. A. Wouthuysen, Phys. Rev. **78**, 29 (1950).

[165] M. Pavšič, Adv. Appl. Clifford Algebras **28**, 89 (2018).

[166] M. V. Polyakov and P. Schweitzer, arXiv:1801.05858 [hep-ph].

[167] M. V. Polyakov and P. Schweitzer, Int. J. Mod. Phys. A **33**, 1830025 (2018).

[168] V. D. Burkert, L. Elouadrhiri, F. X. Girod, C. Lorcé, P. Schweitzer, and P. E. Shanahan, Rev. Mod. Phys. **95**, 041002 (2023), arXiv:2303.08347 [hep-ph].

[169] D. C. Hackett, D. A. Pefkou, and P. E. Shanahan, Phys. Rev. Lett. **132**, 251904 (2024), arXiv:2310.08484 [hep-lat].

[170] H. Shiomi, Nucl. Phys. A **603**, 281 (1996), arXiv:hep-ph/9601329.

[171] E. Leader and C. Lorcé, Phys. Rept. **541**, 163 (2014), arXiv:1309.4235 [hep-ph].

[172] M. Day and K. S. McFarland, Phys. Rev. D **86**, 053003 (2012), arXiv:1206.6745 [hep-ph].

[173] V. Bernard, N. Kaiser, and U. G. Meissner, Phys. Rev. Lett. **69**, 1877 (1992).

[174] A. Liesenfeld *et al.* (A1 Collaboration), Phys. Lett. B **468**, 20 (1999).

[175] R. Petti, R. J. Hill, and O. Tomalak, Phys. Rev. D **109**, L051301 (2024).

[176] N. Kaiser and W. Weise, Phys. Rev. C **110**, 015202 (2024).

[177] J.-Y. Kim and H.-C. Kim, Phys. Rev. D **104**, 074003 (2021), arXiv:2106.10986 [hep-ph].

[178] J.-Y. Kim, Phys. Rev. D **106**, 014022 (2022), arXiv:2204.08248 [hep-ph].

[179] A. Freese and G. A. Miller, Phys. Rev. D **103**, 094023 (2021), arXiv:2102.01683 [hep-ph].

[180] A. Freese and G. A. Miller, Phys. Rev. D **108**, 034008 (2023), arXiv:2210.03807 [hep-ph].

[181] M. Diehl and P. Hagler, Eur. Phys. J. C **44**, 87 (2005), arXiv:hep-ph/0504175.

[182] D. E. Soper, Phys. Rev. D **15**, 1141 (1977).

[183] S. F. Pate, Phys. Rev. Lett. **92**, 082002 (2004), arXiv:hep-ex/0310052.

[184] X.-D. Ji, Phys. Rev. Lett. **78**, 610 (1997).

[185] M. Diehl, Phys. Rept. **388**, 41 (2003), arXiv:hep-ph/0307382.

[186] F. Georges *et al.* (Jefferson Lab Hall A Collaboration), Phys. Rev. Lett. **128**, 252002 (2022), arXiv:2201.03714 [hep-ph].

[187] J. Liang, Y.-B. Yang, T. Draper, M. Gong, and K.-F. Liu (χQCD Collaboration), Phys. Rev. D **98**, 074505 (2018), arXiv:1806.08366 [hep-ph].

[188] P. Reinert, H. Krebs, and E. Epelbaum, Phys. Rev. Lett. **126**, 092501 (2021), arXiv:2006.15360 [nucl-th].

[189] M. L. Goldberger and S. B. Treiman, Phys. Rev. **110**, 1178 (1958).

[190] G. Bardin, J. Duclos, A. Magnon, J. Martino, A. Richter, E. Zavattini, A. Bertin, M. Piccinini, and A. Vitale, Phys. Lett. B **104**, 320 (1981).

[191] V. A. Andreev *et al.* (MuCap Collaboration), Phys. Rev. Lett. **110**, 012504 (2013), arXiv:1210.6545 [nucl-ex].

[192] S. Choi *et al.*, Phys. Rev. Lett. **71**, 3927 (1993).

[193] A. M. Moiseeva and M. V. Polyakov, Nucl. Phys. B **832**, 241 (2010).

[194] J. Y. Panteleeva and M. V. Polyakov, Phys. Rev. D **104**, 014008 (2021).

[195] J.-Y. Kim and H.-C. Kim, Phys. Rev. D **104**, 074019 (2021), arXiv:2105.10279 [hep-ph].

[196] J.-Y. Kim, U. Yakhshiev, and H.-C. Kim, Eur. Phys. J. C **82**, 719 (2022).

[197] P. Choudhary, B. Gurjar, D. Chakrabarti, and A. Mukherjee, Phys. Rev. D **106**, 076004 (2022), arXiv:2206.12206 [hep-ph].

[198] A. Freese and G. A. Miller, Phys. Rev. D **105**, 014003 (2022), arXiv:2108.03301 [hep-ph].

[199] R. N. Bracewell, *The Fourier Transform and Its Applications* (McGraw-Hill, New York, 2000).